In compliance with the
Canadian Privacy Legislation
some supporting forms
may have been removed from
this dissertation.

While these forms may be included
in the document page count,
their removal does not represent
any loss of content from the dissertation.

University of Alberta

Nonlinear Coupled Field Approach to the Finite Element Simulation of Shape Memory Alloy Smart Systems

By

Mohammed Youssef Serry El-Sayed Ahmed

A thesis submitted to the Faculty of Graduate Studies and Research in partial fulfillment of the requirements for the degree of MASTER OF SCIENCE

Department of Mechanical Engineering

Edmonton, Alberta

Fall 2003

National Library of Canada
Acquisitions and Bibliographic Services
395 Wellington Street
Ottawa ON K1A 0N4
Canada

Bibliothèque nationale du Canada
Acquisisitons et services bibliographiques
395, rue Wellington
Ottawa ON K1A 0N4
Canada

Your file Votre référence
ISBN: 0-612-87705-1
Our file Notre référence
ISBN: 0-612-87705-1

The author has granted a non-exclusive licence allowing the National Library of Canada to reproduce, loan, distribute or sell copies of this thesis in microform, paper or electronic formats.

The author retains ownership of the copyright in this thesis. Neither the thesis nor substantial extracts from it may be printed or otherwise reproduced without the author's permission.

L'auteur a accordé une licence non exclusive permettant à la Bibliothèque nationale du Canada de reproduire, prêter, distribuer ou vendre des copies de cette thèse sous la forme de microfiche/film, de reproduction sur papier ou sur format électronique.

L'auteur conserve la propriété du droit d'auteur qui protège cette thèse. Ni la thèse ni des extraits substantiels de celle-ci ne doivent être imprimés ou aturement reproduits sans son autorisation.

Canadä

UNIVERSITY OF ALBERTA

LIBRARY RELEASE FORM

Name of Author: Mohammed Youssef Serry El-Sayed Ahmed

Title of Thesis: Nonlinear Coupled Field Approach to the Finite Element Simulation of Shape Memory Alloy Smart Systems

Degree: Master of Science

Year this Degree Granted: 2003

Permission is hereby granted to the University of Alberta Library to reproduce single copies of this thesis and to lend or sell such copies for private, scholarly or scientific research purposes only.

The author reserves all other publication and other rights in association with the copyright in the thesis, and except as herein before provided, neither the thesis nor any substantial portion thereof may be printed or otherwise reproduced in any material form whatever without the author's prior written permission.

May 15th 2003

UNIVERSITY OF ALBERTA

FACULTY OF GRADUATE STUDIES AND RESEARCH

The undersigned certify that they have read, and recommend to the Faculty of Graduate Studies and Research for acceptance, a thesis entitled "Nonlinear Coupled Field Approach to the Finite Element Simulation of Shape Memory Alloy Smart Systems" submitted by Mohammed Youssef Serry El-Sayed Ahmed in partial fulfillment of the requirements for the degree of Master of Science.

Dr. V

Dr. Dona

Dr. Dongyang Li

Date: May 7th 2003

ABSTRACT

In this dissertation, we addressed the issue of the finite element simulation of Shape Memory Alloy (SMA) smart systems.

This is done in two main parts. The first part involves developing a general finite element procedure for modeling SMA smart systems. The main characteristics of the is its suitability for modeling multi-field smart systems' applications (e.g. subjected to electro-thermo-structural loading and boundary conditions) that incorporate SMA components its ability to model various types of nonlinearity whether they're due to large deformations or due to SMA material functions. The procedure was validated by comparing experimental and numerical results obtained from the literature with results of the finite element procedure.

The second part of the research involves utilizing the developed procedure to simulate a self-damage control SMA smart system. The study aimed at investigating the effect of changing various parameters of the smart system on its crack closing efficiency, and hence, characterizing the performance of the smart system.

ACKNOWLEDGMENT

My sincere thanks and gratitude to my supervisors, Dr. Walied Moussa and Dr. Don Raboud for their timely advice, patience and valuable guidance throughout the period of research leading to this dissertation. This work has been supported by funding from National Sciences and Engineering Research Council of Canada.

Lastly my sincerest thanks and appreciation to my parents Mr. Youssef Serry and Mrs. Tayseer AbdelFatah, my parents in law Dr.Othman El-Sayed and Dr.Sanaa Ahmed and my wife Rasha Othman for bearing with all my tantrums and insanity for the past two years.

TABLE OF CONTENTS

1 Introduction ---- 1

2 Literature Review

2.1 Background of SMA ---- 5

2.1.1 Shape Memory Effect ---- 6

2.1.2 SMA. Pseudoelasic Behavior ---- 6

2.2 Constitutive Modeling of SMA ---- 7

2.3 Finite Element Modeling of SMAs ---- 10

2.4 SMA-embedded-wires Composite ---- 11

2.5 Linear Elastic Fracture Mechanics Background ---- 13

2.5.1 Historical Overview of LEFM ---- 13

2.5.2 LEFM Assumptions ---- 14

3 Finite Element Modeling of SMA Smart Systems

3.1 SMA Finite Element Structural Frame Work ---- 21

3.2 SMA Finite Element Thermo-Electrical Frame Work ---- 25

3.3 Solution Procedure ---- 27

3.4 Validation of the Numerical Results and Discussion ---- 29

3.4.1 Validation of the Electro-thermal Procedure ---- 30

3.4.2 Validation of the Thermo-structural Procedure ---- 31

3.4.3 Validation of the Shape Memory Effect ----32

3.5 Concluding Remarks and Summary of the FEM Procedure ---- 33

4. FE analysis of the behavior of a SMA self-damage-control Smart System

4.1 Smart System's Simulation and Development ---- 40

4.2. Modeling and Assumptions ---- 41

4.2.1 SMA Wires Sensing/Actuating Mechanisms ---- 42

4.2.2 SMA Nonlinear Structural Finite Element Derivation ---- 43

4.2.3 SMA Electro-thermal Finite Element Derivation ---- 43

4.2.4 Two-dimensional Thermo-Structural Finite Element Derivation ---- 44

4.2.5 Crack-tip Stress Intensity Factor ---- 44

4.2.6 SMA Wires Material Properties Evolution Functions ---- 45

4.3. Model Description and Solution Procedure ---- 45

4.4.Application and Discussion ---- 47

4.4.1 Smart System Sensing/Actuating Response ---- 47

4.4.2 Parametric Study ---- 48

4.5 Concluding Remarks ---- 55

5. Conclusions and Future Work

5.1 Conclusions ----72

5.2 Future Work ----75

Bibliography ---- 77

Appendix

A1- Expressions of the Symbols in Equation (3.2) ---- 90

A2- Derivation of the Term ${}^{t}C_{ijrs}$ Using Brinson (1993) Modified Constitutive and Kinetic Relations ----91

A3- Derivation of $\left[\frac{\partial \xi}{\partial \sigma} \; \frac{\partial \xi_s}{\partial \sigma} \right]$ for Different Types of SMA Transformation ----92

A4- Expressions of the Symbols in Equation (3.14) ---- 93

A5- Kinetic Relations Used by Amalraj et al for Modeling SMA Behavior ----94

A6- SMA Material Properties Functions ---- 94

A7- Out-of-balance Load Vector Convergence Criterion ----95

LIST OF TABLES

Table 3.1 SMA properties for different numerical & experimental verification problems ---35

Table 4.1 Unchanged properties for various cases ---57

Table 4.2 Different linear isotropic materials used for the effect of matrix material case study ---57

Table 4.3 Phases of different SMA wire states in Figure 4.4 ---58

LIST OF FIGURES

Figure 2.1 Different phases of an SMA. ---17

Figure 2.2 Temperature-induced phase transformation of an SMA without mechanical loading. ---17

Figure 2.3 Shape Memory Effect of an SMA. ---18

Figure 2.4 Pseudoelastic loading path. ---18

Figure 2.5 Pseudoelastic stress-strain diagram ---19

Figure 2.6 Location of local stresses near a crack tip in cylindrical coordinates. ---19

Figure 2.7 Three loading modes ---20

Figure 2.8 Stress Intensity factor for (a) center cracked plate loaded in tension, (b) edge cracked plate loaded in tension ---20

Figure 3.1 Nonlinear Coupled field solution procedure ---36

Figure 3.2 Temperature distribution along SMA wire after 10 sec., applying Convection, Isothermal and Adiabatic boundary conditions at the end ---37

Figure 3.3 Stress –strain curve obtained by loading SMA wire at strain rate of 6.4e-5 and convection in air ---37

Figure 3.4 Stress –strain curve obtained by loading SMA wire at strain rate of 6.4e-4 and convection in air ---38

Figure 3.5 Stress –strain curve obtained by loading SMA wire at strain rate of 6.4e-3 and convection in air ---38

Figure 3.6 Stress --strain curve obtained by loading SMA at T=263 K (Below martensite start temperature) ---39

Figure 4.1 Crack Control Smart Composite System ---59

Figure 4.2 Profile, Front and Crack views of the model ---59

Figure 4.3 An SMA self damage control composite working as smart-bond between a patch and the aircraft skin ---60

Figure 4.4 Schematic diagram of the SMA wires stress-temperature loading ---60

Figure 4.5 Schematic diagram of the system showing the constrained axes in the vertical and horizontal directions and the mesh ---61

Figure 4.6 SMA martensite volume fraction versus SIF of the crack, for different cracks ---61

Figure 4.7 Typical SMA wires stress difference - temperature difference loading diagram ---62

Figure 4.8 Crack tip shape at the different temperatures at Current density of 6 amp/mm2 ---62

Figure 4.9 Time versus stress intensity factor at different current densities ---63

Figure 4.10 Effect of Increasing Current Density in the SMA wires on the SIF at different temperatures. ---63

Figure 4.11 Rate of Temperature rise versus SIF at different current densities ---64

Figure 4.12 SIF of the crack versus Time at different wires' diameter, wires actuated at 0.25 amps. ---64

Figure 4.13 Schematic diagram of showing different number of actuated wires per crack ---65

Figure 4.14 Temperature difference of the wire versus stress intensity factor at different number of activated wires ---65

Figure 4.15 Average martensite volume fraction of the wires versus stress intensity factor for different number of activated wires ---66

Figure 4.16 Maximum SIF and stress per wire versus applied stresses ---66

Figure 4.17 Temperature difference of the wires versus stress intensity factor for different applied stress ---67

Figure 4.18 Time versus stress intensity factor for different wire prestrain ---67

Figure 4.19 Effect of increasing SMA wire prestrain on the SIF after different times. ---68

Figure 4.20 Martensite volume fraction of the wires versus stress intensity factor for different wire prestrains ---68

Figure 4.21 Time versus stress intensity factor at different heat convection coefficients ---69

Figure 4.22 Time versus stress intensity factor at different heat convection coefficients ---69

Figure 4.23 Initial system's temperature versus stress intensity factor ---70

Figure 4.24 Temperature difference of the wires versus stress intensity factor for different matrix materials ---70

Figure 4.25 Martensite volume fraction rate of change versus time for different materials ---71

LIST OF SYMBOLS

ε_{ij}	---Total strain components.
σ_{ij}	---Applied stress components.
V	---Initial volume.
ξ	---Martensite volume fraction.
J	---Applied current density.
θ_i	---Nodal temperature vector.
θ_{amb}	---Ambient temperature.
K_L	---Linear stiffness matrix.
K_{NL}	---Nonlinear stiffness matrix.
ΔU	---Displacement Increment
$\Re$	---External loading vector.
${}^{t}F$	---Internal forces due to stresses
B_L	---Liner strain-deformation matrix.
B_{NL}	---Nonlinear strain-deformation.
S	---Stress vector.
H	---Shape functions matrix.
H^S	--- Surface shape function matrix.
C_{ijrs}	---Stress-strain matrix.
D	---Young's modulus.

D_a ---Austenitic young's modulus.

D_m ---Martensitic young's modulus.

Ω ---SMA transformation vector.

ξ_s ---Stress induced martensite volume fraction.

ξ_θ ---Temperature induced martensite volume fraction.

α ---Stress induced due to temperature effect.

σ_s^{cr} ---SMA starting critical stress.

σ_f^{cr} ---SMA finishing critical stress.

Q_l ---Latent heat due to phase transformation.

ε_L ---Maximum shape memory strain

$\dot{\xi}$ ---MVF rate of change with time.

K^k ---Heat conductivity matrix.

K^c ---Heat convection matrix

Q^c ---Vector of convection heat power input

Q^k ---Vector of conduction heat power input

C ---Heat capacity matrix

$\tilde{Q}$ ---Vector of total concentrated heat input

ρ_A ---Austenitic SMA electrical resistivity

ρ_M ---Martensitic SMA electrical resistivity

ε_{ij}^{th} ---Thermal strain components.

C_r ---Stress-Strain relationship matrix.

θ_o	---Initial temperature vector.
H_{ri}	---2D polymeric matrix Element's shape functions
ν	---Poisson's ratio.
α_r	---Polymeric matrix CTE
E_r	---Polymeric matrix modulus of elasticity
KI	--- Stress Intensity Factor
M_S	---Martensite start temperature
M_F	---Martensite finish temperature
A_S	---Austenite start temperature
A_F	---Austenite finish temperature
$S_{M \longrightarrow A}$	---Is the standard deviation of the normal distribution of the SMA kinetic model.
a_l , a_k	--- General finite element nodal degrees of freedom.
P	---Electrical power

1. Introduction

Smart systems are systems that augment the computational ability of microelectronics with the perception and control abilities of sensors and actuators. They are usually characterized by the interaction of components operating on different physical domains (i.e. structural, thermal or electrical domains). The analysis of such complex systems requires the modeling and simulation of single components as well as the overall system.

Shape Memory Alloys are widely used in a variety of smart systems' applications such as in MEMS and SMA embedded wires in composites smart systems. They've been attractive for MEMS applications because of their ability to provide an integrated micro-actuation and micro-sensing mechanisms that is compatible with micro-fabrication, and to provide a large displacement and a large actuation energy density. In MEMS applications, SMAs have been used as micro-actuators (Walker et al, 1990), micro-valves (Bush and Johnson, 1990 and Ray et al, 1992), thermo-mechanical switches (Kim et al, 1995), micro-actuators used for robotic manipulators (Kuribayashi and Taniguchi, 1992), normally closed micro-valves and micro-pumps (H Khan et al, 1998).

SMA-embedded composites smart structures have become very attractive in the development of novel actuators, sensors and adaptive systems. Their applications may significantly improve the performance of various aerospace systems such as aircraft wings, rotor blades, engine nozzles and air inlets. They've been used for active control of sound radiation (Saunders et al, 1991), direct in-flight incremental adjustment in helicopter rotor blades (Giurgiutiu et al, 1997 and Prahlad et al , 2000), to modify flutter

instability boundaries of the plate subjected to supersonic flow (Ostachowicz et al, 2001) and as adaptive composites to adjust resonance vibration frequency (Balta et al, 2001).

Therefore, for smart systems involving SMA components, the ability to accurately model and analyze these structures is extremely important for several reasons. The high cost of the fabrication processes which could be significantly decreased by the incorporation of the SMA finite element procedure into the design stages of new products, and the properties of the SMA component in a given design can be varied systematically in analysis with specially tailored properties that will realize their full potential in each individual application.

However, due to the nature of most of smart systems' applications which require the incorporation of different working fields at the same time (e.g. mechanical, thermal and electrical fields), and due to the nature of the shape memory alloys unique material properties (e.g. variable electrical resistivity, thermal conductivity, etc.), and mechanical behaviors (e.g. shape memory and pseudoelasic effects), which all make the modeling of these applications a highly nonlinear and coupled problem.

To date, finite element procedures developed to consider applications with shape memory alloys work well for the problems for which they were developed. However, a general approach, which works well for a variety of applications, especially in smart systems' areas, and is capable of incorporating the complex behavior associated with shape memory alloys and coupled field theories, is still missing from the literature.

In this dissertation we apply a nonlinear coupled field finite element procedure to simulate the behavior of SMA components used in smart systems' applications. The goal is to introduce a general purpose finite element procedure that is capable of capturing

mechanical and thermal phase transformations and to be able to model applications containing SMAs subjected to electro-thermo-mechanical loading with variable SMA material properties assumed, as well as large mechanical deformations and nonlinear heat transfer conditions.

The key feature of the proposed procedure is that it built on two basic finite element procedures, the nonlinear structural and the nonlinear transient electro-thermal procedures; the procedures are based on the concepts of continuum mechanics, so they could be easily adapted in the modeling stage to integrate with a wide variety of SMA constitutive models, kinematical relations (based on the geometry), and multi-dimensional problems. In the solution stage, the idea of multiphysics is revisited by solving different loading schemes in a sequential way, and then combines them together after each iteration.

We hope that this procedure will introduce a general finite element tool for modeling of variety of smart systems without being constrained with the geometry (e.g. beam, wire, or membrane), shape (one-dimensional or multi-dimensional), material constitutive law, variability in material properties or type of loading (e.g. mechanical, thermal or electrical).

The second part of this work deals with the simulation of a self-damage control smart system which consists of SMA wires embedded in a polymeric matrix. A novel self damage control smart system is proposed and simulated, and a parametric study of the behavior of this system is performed. Simulation and modeling is performed using the finite element method, and new 1-D nonlinear SMA structural and electro-thermal elements were developed for this purpose. Also, a thermo-structural linear isotropic

element is used to model the polymeric matrix material. The proposed system is characterized by its ability to monitor the system for cracks continuously, and to actuate the SMA wires to close the crack and to minimize the risk of structure failure.

2. Literature Review

In this chapter we review and introduce some theoretical background of the SMA and the application modeled in this dissertation.

2.1 Background of SMA (Phase Transformation and Mechanical Behavior)

Shape Memory Alloys are a unique class of metal alloys that can recover apparently permanent strains when they are heated above a certain temperature.

SMAs have two stable phases - the high-temperature phase, called austenite and the low-temperature phase, called martensite. In addition, the martensite can be in one of two forms: twinned and detwinned, as shown in Figure 2.1. The basis for the unique properties of the SMAs is a phase transformation that occurs between these two phases upon heating or cooling. The key effects of SMAs associated with the phase transformation are pseudoelasticity and the shape memory effect.

Upon cooling and in the absence of applied load, the material transforms from austenite into twinned martensite. As a result of this phase transformation no observable macroscopic shape change occurs. Upon heating the material in the martensitic phase, a reverse phase transformation takes place to austenite. The above process is shown in Figure 2.2, in which four characteristic temperatures are defined:

- Martensitic start temperature (M_S), which is the temperature at which, the material starts transforming from austenite to martensite; upon cooling.
- Martensitic finish temperature (M_F), at which the transformation is complete and the material is fully in the martensitic phase;
- Austenite start temperature (A_S) at which the reverse transformation (austenite to martensite) initiates; upon heating.
- And, austenite finish temperature (A_F) at which the reverse phase transformation is completed and the material is the austenitic phase.

2.1.1 Shape Memory Effect

If a mechanical load is applied to the material in the state of twinned martensite (at low temperature) it is possible to *detwin* the martensite. Upon releasing the load, the material remains deformed because the forms of martensite are similar. A subsequent heating of the material to a temperature above A_F will result in a complete reverse phase transformation (martensite to austenite) and will lead to complete shape recovery, as shown in Figure 2.3. The above described process results in manifestation of the *Shape Memory Effect* (SME).

2.1.2 SMA. Pseudoelastic Behavior

It is also possible to induce a phase transformation at a certain temperature by applying a pure mechanical load. The result of this load application is fully detwinned martensite and very large strains are observed. If the temperature of the material is above A_F but only to a certain point, a complete shape recovery is observed upon

unloading, thus, the material behavior resembles elasticity however its highly nonlinear with hysteresis effects. The above-described effect is known under the name of *Pseudoelastic Effect*. A loading path demonstrating the pseudoelasic effect is schematically shown in Figure 2.4, while the resulting stress-strain diagram is shown in Figure 2.5.

2.2 Constitutive Modeling of SMA

Various approaches have been taken by researchers thus far to develop SMA constitutive models: macroscopic, microscopic, and mixed. In the macroscopic approach, the constitutive model describes the material behavior based on experimental data. For the microscopic approach, the constitutive model attempts to predict and describe the material behavior based on fundamental physical concepts, such as the microstructure of the crystal lattice (Liang et al., 1990). Finally, the mixed approach uses a combination of both microscopic and macroscopic concepts for better modeling.

Models proposed by many researchers have been classified in five different types: ferroelectrics model (Müller et al, 1979,1980,1989,1991), internal variable model (Liang and Rogers, 1990), plasticity model (Kafka, 1994), hysteresis model (Graesser and Cozzarelli, 1990, 1991) and non-isothermal model (Ivshin and Pence, 1994) and (Pence et al, 1994).

Internal variable models have been the most suitable for engineering applications, and many developments on this model has been reported in literature. This model is derived from the concept of the Helmholtz free energy, which can be derived from thermodynamic principles. The Helmholtz free energy is a function of the general state variable Λ. The state variables for shape memory alloys are defined as strain (ε),

temperature (θ) , and martensite fraction (ζ). Thus, the general state variable can be defined as:

$$\Lambda = (\varepsilon, \theta, \zeta). \tag{2.1}$$

Based on Equation (2.1), the constitutive relation can be derived by using the first and second laws of thermodynamics (Liang and Rogers, 1990) from which, the rate form of the constitutive equation which describes the change of stress in terms of strain, temperature and martensite fraction can be derived as:

$$\sigma = D\, d\varepsilon + \Theta\, dT + \Omega\, d\zeta\,, \tag{2.2}$$

where D is the Young's modulus, Θ is the thermoelastic tensor, and Ω is the transformation tensor, which defines the change of strain during the phase transformation. If the equation of free energy is specified, the equilibrium state of phases can be obtained by minimizing the free energy. Thus, the relation among the martensite fraction, the applied stress and temperature can be obtained. However, it is impractical to obtain such an equation. Instead of deriving the equation of free energy, the martensite fraction (ζ) is assumed to be function of stress and temperature and experimental data is used to fit the martensitic transformation or austenitic transformation relations. Considering different functions of martensite transformation fraction, many researchers developed different internal variable models.

Further work has been done on this model was later extended to 3-D SMA model (Liang and Rogers, 1992). The 3-D model can be applied in studying complex structures

made of shape memory alloys. The model was also extended to be capable of predicting two-way shape memory effect (Zhang et al, 1992).

Brinson (1993) developed another cosine model based on Liang and Rogers's model. In this model, the martensite fraction internal variable is separated into stress-induced and temperature-induced components:

$$\zeta = \zeta_S + \zeta_\theta \qquad (2.3)$$

Where (ζ_θ) is the martensite fraction of SMA which is induced by temperature with multiple variants, and (ζ_S) is the martensite fraction of SMA, which is oriented by stress into a single martensite variant. By separating these two components, the model can predict and describe stress-induced martensitic transformation at temperatures above As for superelastic behaviors, and predict and describe the shape memory effect with applied stress at all temperatures. Thus, Brinson's model is applicable over a large range of temperatures. Non-constant material functions, which account for the change of material properties, were also introduced in Brinson's model. By using common and measurable material properties, Brinson's model can be easily used in engineering design and for computations of the stress-strain relations and the superelastic effects of SMA.

The model proposed by Brinson accomplishes the following advantages:

- Capable of predicting the behavior of the system under *variable* mechanical or thermal loads.
- Capable of predicting shape memory and pseudoelastic behaviors.
- Taking into consideration the stress history.
- Using common measurable material properties.

2.3 Finite Element Modeling of SMAs

Finite element modeling of SMA has been extensively considered in literature. Brinson and Lammering (1993) presented a displacement based one-dimensional isothermal nonlinear finite element procedure that is capable of capturing the pseudoelasticity and the shape memory effect of the SMA. The model concentrated on stress-induced phase transformation of SMAs and utilized the continuum mechanics incremental equation of motion to model nonlinearties of the system due to large deformations. The transient model could successfully simulate the active frequency control of a composite strip with embedded SMA wires.

Wu (1996) used finite element methods to solve a nonlinear transient system of equations of a thermally driven shape memory alloy plate bonded to a matrix of elastomer under uniform distributed load.

Ferdinando et al (1997) introduced a model known as generalized plasticity, which was adopted as a framework for the development of one- and three-dimensional constitutive models for shape memory alloys. The model was implemented in a finite element scheme for isothermal conditions. Numerical simulations of uniaxial loading and three- and four-point bending tests were performed and compared to the available experimental data with good agreement.

Trochu and Qian (1997) also presented a nonlinear finite element procedure to simulate the pseudoelasticity of SMAs, based on a newly formulated and simplified constitutive law derived from the plastic flow theory. The procedure has been validated for isothermal uniaxial and beam problems.

Auricchio et al (1999) presented a thermomechanical one-dimensional constitutive model based on the use of strain and temperature as control variables. The model was implemented in a small-deformation beam finite element which was used to simulate the tensile, pure bending and three point bending tests and orthodontic wires.

Amalraj el al (2000) presented a finite element modeling of the temperature distribution in a SMA wire with variable material properties. This was done by modeling the transformation of an electrically heated initially martensitic wire under zero stress conditions. The model accounts for an evolution in the thermal conductivity, electrical resistivity, and heat capacity during the phase transformation.

Stoilov et al (2000) proposed the moving boundary finite element method -based numerical approach to solve one-dimensional thermo-mechanical problems in shape memory alloys with a moving phase boundary. The approach was demonstrated to be accurate and unconditionally stable.

2.4 SMA-embedded-wires Composite

Recently, shape-memory-alloys-embedded composite smart structures have become very attractive in the development of novel actuators, sensors and adaptive systems.

Their application may significantly improve the performance of various aerospace systems such as aircraft wings, rotor blades, engine nozzles and air inlets. Efforts to investigate the behavior and to utilize the potentials of SMA-smart composites could be tracked to the year 1993; work in this area can be categorized into five main categories. The first category is the work concerned with simulating and studying the mechanical

behavior of SMA smart composites, in this essence DeBlonk et al (1995) presented a framework for the identification of the constitutive law for a class of nonlinear models of shape-memory-alloy-embedded elastomeric rods. Other work under this category has been done by Hebda et al (1995), Bruck et al (1999), Lurie et al (2000) and many others.

The second category deals with the dynamic responses of SMA-composite structures, such the work done by Boller et al (2001), which discusses the hysteresis between transformation to martensite and austenite in a SMA as an intrinsic material property to be used to enhance damping of a shape memory alloy composite. The work done by Zheng et al (2001) studied the effect of partial cycling on the reverse martensitic transformation of TiNi fibers embedded in a cement composite.

Other work was mainly devoted to the applications of the SMA smart composites such as Liang et al (1991) who presented a theoretical analysis of sound transmission/radiation of SMA hybrid composite panels. Saunders et al (1991) demonstrated active control of sound radiation from a clamped, baffled, composite beam with embedded SMA fibers. Paine et al (1995) addressed utilizing the SMA's substantial capacity to dissipate strain energy to increase the hybrid composite's static functionality. Giurgiutiu et al (1997) utilized a composite consisting of shape memory alloy wires embedded into a polymeric matrix as a material for helicopter rotors blades for achieving direct in-flight incremental adjustment of the tracking tab.

Some works were only concerned with the fabrication of these composites, such as the work done by Wei et al (1997) who overviewed the principles, the basic design concepts and the fabrication of SMA composites. Ya et al (2002) developed a new

method for to fabricate SMA/CFRP smart composites without using special fixture jugs by controlling the transformation temperatures of SMA during fabrication.

And finally, efforts to investigate the self-damage control ability of the SMA smart composites are quite recent and rare. The work done by Byung et al (1999) who investigated manufacturing and experimental thermomechanical characterization and effect of damage recovery on the pre-strained SMA wires embedded CFRP composites for developing smart composite with self-damage control. Wang et al (2002) who described the modeling of a cracked structure repaired by SMA wire-reinforced composite patches and further evaluated the active closure stress.

2.5 Linear Elastic Fracture Mechanics Background

Linear elastic fracture mechanics (LEFM) principles are used to relate the stress magnitude and distribution near the crack tip to:

- Remote stresses applied to the cracked component
- The crack size and shape
- The material properties of the cracked component

2.5.1 Historical Overview of LEFM

In the 1920s, Griffith formulated the concept that a crack in a component will propagate if the total energy of the system is lowered with crack propagation. That is, if the change in elastic strain energy due to crack extension is larger than the energy required to create new crack surfaces, crack propagation will occur. Griffith's theory was developed for brittle materials. In the 1940s, Irwin extended the theory for ductile

materials. He postulated that the energy due to plastic deformation must be added to the surface energy associated with the creation of new crack surfaces. He recognized that for ductile materials, the surface energy term is often negligible compared to the energy associated with plastic deformation. Further, he defined a quantity, G, the strain energy release rate or "crack driving force," which is the total energy absorbed during cracking per unit increase in crack length per unit thickness. In the mid-1950s, Irwin made another significant contribution. He showed that the local stresses near the crack tip are of the general form

$$\sigma_{ij} = \frac{KI}{\sqrt{2\pi r}} f_{ij}(\theta) + (higher\ order\ terms)$$

(2.4)

Where r and θ are cylindrical coordinates of a point with respect to the crack tip (see Figure 2.6) and KI is the stress intensity factor. He further showed that the energy approach (the "G" approach above) is equivalent to the stress intensity approach and that crack propagation occurs when a critical strain energy release rate, G, (or in terms of a critical stress intensity, KI) is achieved.

2.5.2 LEFM Assumptions

Linear elastic fracture mechanics is based on the application of the theory of elasticity to bodies containing cracks or defects. The assumptions used in elasticity are also inherent in the theory of LEFM: small displacements and general linearity between stresses and strains. The general form of the LEFM equations is given in Equation 2.4. As seen, a singularity exists such that as *r*, the distance from the crack tip, tends toward zero, the stresses go to infinity. Since materials plastically deform as the yield stress is

exceeded, a plastic zone will form near the crack tip. The basis of LEFM remains valid, though, if this region of plasticity remains small in relation to the overall dimensions of the crack and cracked body.

There are generally three modes of loading, which involve different crack surface displacements (see Figure 2.7). The three modes are:

- Mode 1: Opening or tensile mode (the crack faces are pulled apart).
- Mode 2: Sliding or in-plane shear (the crack surfaces slide over each other).
- Mode 3: Tearing or anti-plane shear (the crack surfaces move parallel to the leading edge of the crack and relative to each other).

The following discussion deals with Mode 1 since this is the predominant loading mode in the current application. Similar treatments can readily be extended to Modes 2 and 3.

The stress intensity factor, KI, which was introduced in Equation 2.5, defines the magnitude of the local stresses around the crack tip. This factor depends on loading, crack size, crack shape, and geometric boundaries, with the general form given by:

$$KI = \sigma\sqrt{\pi a}\, f\left(\frac{a}{w}\right) \tag{2.5}$$

Where σ is the remote stress applied to component (not to be confused with the local stresses, σ_{ij}, in Equation 2.4), a is the crack length and $f(a/w)$ is the correction factor that depends on specimen and crack geometry. Figure 2.8 gives the stress intensity relationships for a few of the more common loading conditions. Stress intensity factors

for a single loading mode can be added algebraically. Consequently, stress intensity factors for complex loading conditions of the same mode can be determined from the superposition of simpler results, such as those readily obtainable from handbooks.

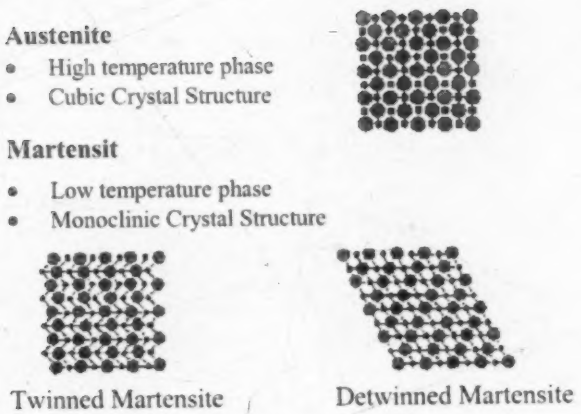

Figure 2.1: Different phases of an SMA. (http://smart.tamu.edu).

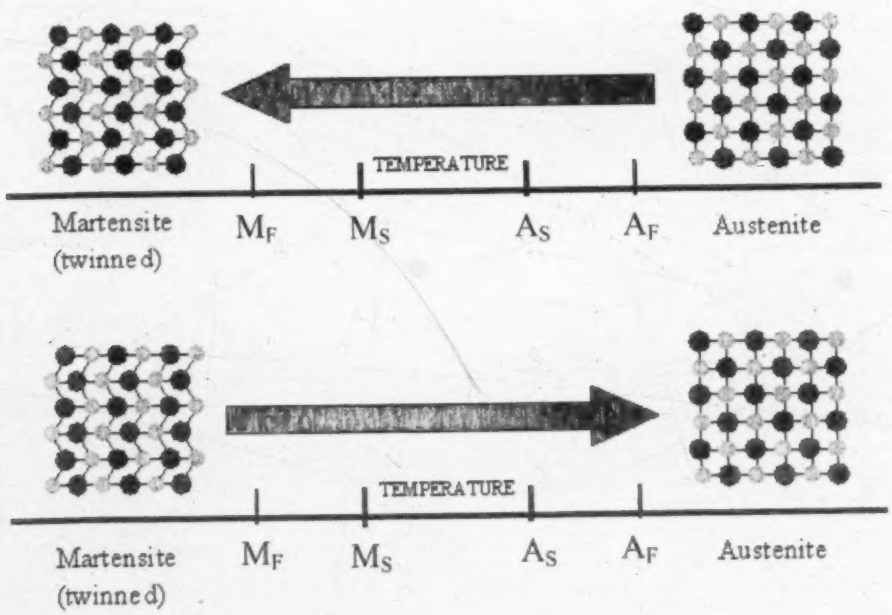

Figure 2.2: Temperature-induced phase transformation of an SMA without mechanical loading. (http://smart.tamu.edu).

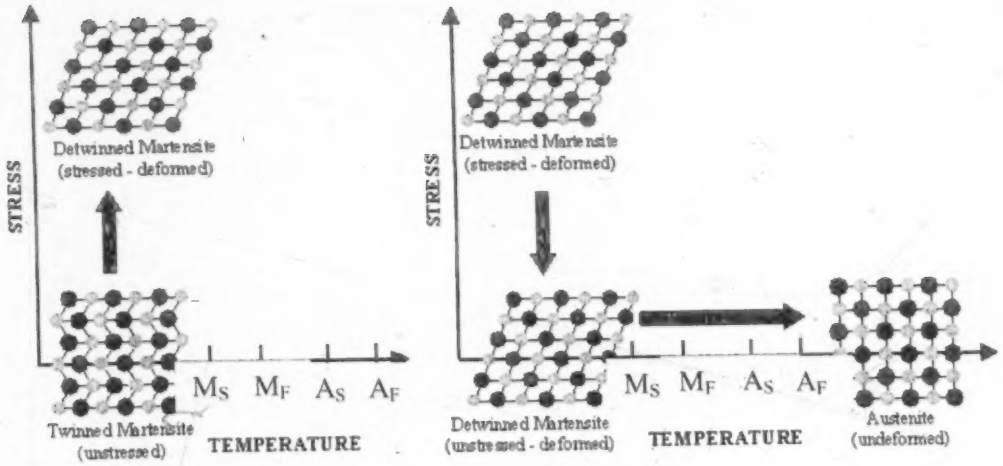

Figure 2.3: Shape Memory Effect of an SMA. (http://smart.tamu.edu).

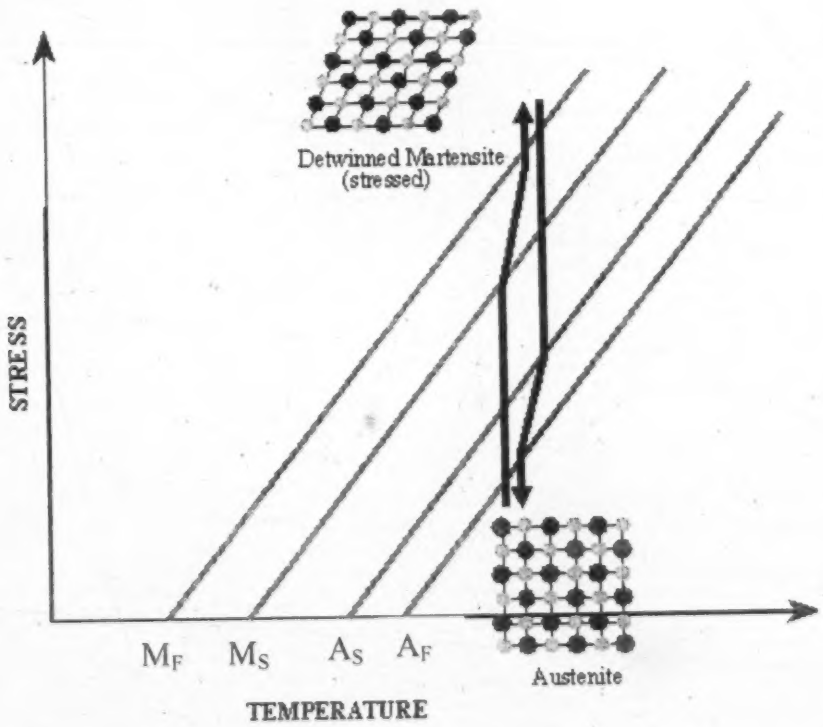

Figure 2.4: Pseudoelastic loading path. (http://smart.tamu.edu).

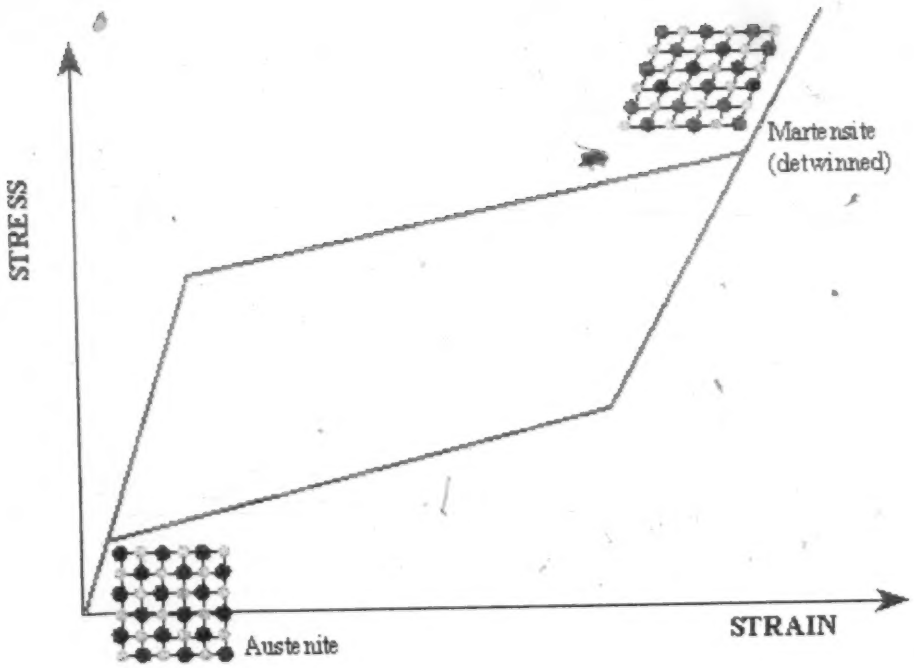

Figure 2.5: Pseudoelastic stress-strain diagram (http://smart.tamu.edu).

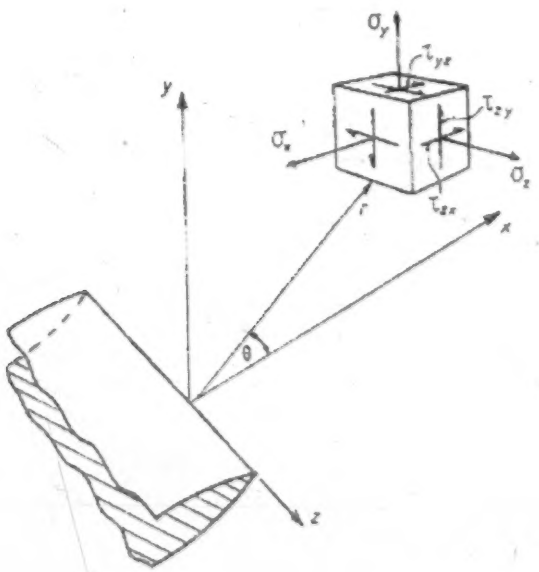

Figure 2.6: Location of local stresses near a crack tip in cylindrical coordinates.

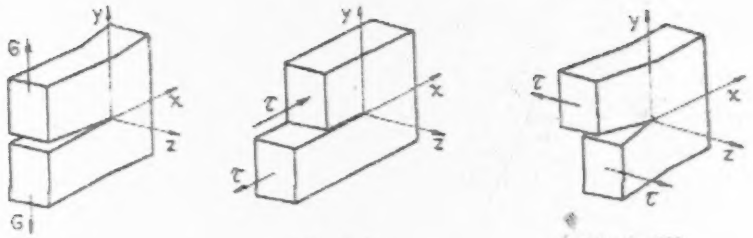

Figure 2.7: Three loading modes.

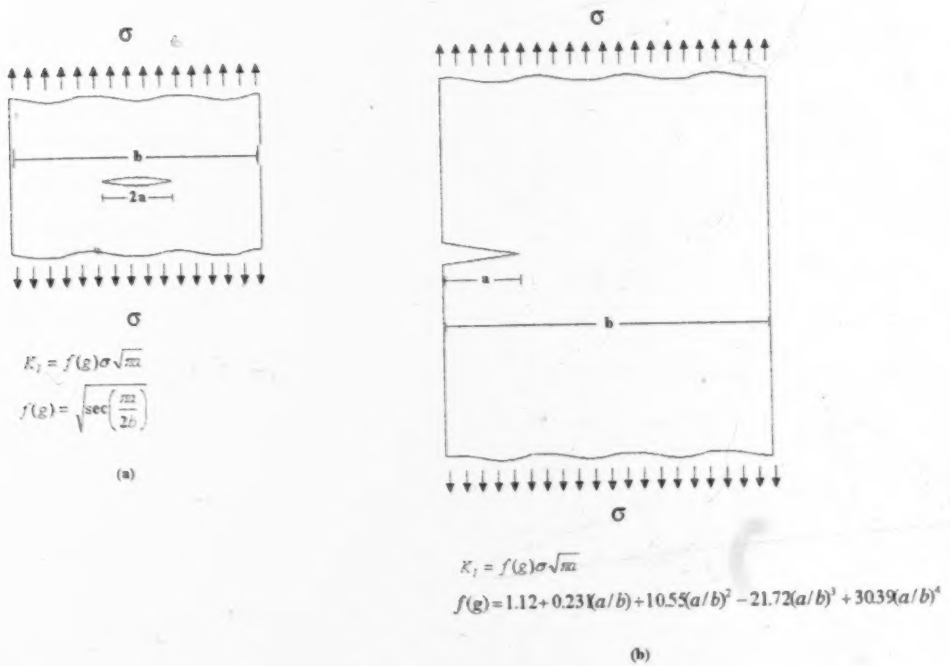

Figure 2.8: Stress Intensity factor for (a) center cracked plate loaded in tension, (b) edge cracked plate loaded in tension.

3. Finite Element Modeling of SMA Smart Systems

In this chapter, we report the development of a general finite element procedure for modeling smart systems applications containing SMA components. The procedure is based on the coupled field finite element concept and it suitable for modeling SMAs subjected to electro-thermo-structural loading.

3.1 SMA Finite Element Structural Frame Work

One of the main reasons for using SMA components in smart systems is their ability to have large elastic strain up to 8%. Therefore, any general finite element procedure for modeling these components should take into consideration nonlinearity due to the possibility of large deformations and large strains, as well as the material nonlinearity. As a result, stresses and strains should be incremented for each time step in this case, and therefore, the linearized form of the virtual work should be used (Bathe, 1996).

In order to obtain such expressions we followed Bathe (1996), by applying the principle of virtual displacement on the total Lagrangian formulation, then linearizing using a Taylor series. Utilizing the definition of the Green-Lagrange strain results in the linearized virtual work expression:

$$\left[\int_{{}^{o}V} C_{ijrs} \frac{\partial\, {}^{t}\varepsilon_{rs}}{\partial\, {}^{t}a_k} \frac{\partial\, {}^{t}\varepsilon_{rs}}{\partial\, {}^{t}a_l} d^{o}V + \int_{{}^{o}V} {}^{t}\sigma_{ij} \frac{\partial^2\, {}^{t}\varepsilon_{rs}}{\partial\, {}^{t}a_k \partial\, {}^{t}a_l} d^{o}V \right] \delta a_l\, da_k \tag{3.1}$$

$$= {}^{t+\Delta t}\Re - \left[\int_{{}^{o}V} {}^{t}\sigma_{ij} \frac{\partial\, {}^{t}\varepsilon_{ij}}{\partial\, {}^{t}a_l} d^{o}V \right] \delta a_l$$

Putting the above expression in terms of stiffness matrices and force and deformation vectors gives:

$$({}^{t}K_{L}^{(i-1)} + {}^{t}K_{NL}^{(i-1)})\,\Delta U^{(i)} = {}^{t+\Delta t}\Re - {}^{t}F^{(i-1)}. \tag{3.2}$$

Note that the left superscripts indicate the time step in which the configuration occurs, while, the right superscripts indicate the Newton-Raphson iteration index.

Expressions for the above symbols are given for *m* number of elements in Appendix A1; we will mention here the expression of the linear stiffness matrix because of its importance in the subsequent derivations:

$${}^{t}K_{L}^{(i-1)} = \sum_{m} \int_{{}^{o}V} {}^{t}B_{L}^{(m)(i-1)T}\ {}^{t}C^{(m)(i-1)}\ {}^{t}B_{L}^{(m)(i-1)}\, d^{o}V, \tag{3.3}$$

in the above expression, the stress- strain relation matrix, ${}^{t}C$, defined as ${}^{t}C_{ijrs} = \dfrac{\partial\, {}^{t}\sigma_{ij}}{\partial\, {}^{t}\varepsilon_{rs}}$ for the SMA element should be determined at each time step. In order to do that; specific SMA constitutive model will be used.

For this model, any of the SMA constitutive relations available in literature might be utilized to get the $\dfrac{\partial\, {}^{t}\sigma_{ij}}{\partial\, {}^{t}\varepsilon_{rs}}$ at any time step, *t*. As an example, we will derive the above expression using the SMA constitutive and kinetic models presented first by Tanaka (1986) modified by Brinson (1993), which is based on the energy balance equations. The relation used is,

$$\sigma - \sigma_{o} = D(\xi)\varepsilon - D(\xi_{o})\,\varepsilon_{o} + \Omega(\xi)\,\xi_{s} - \Omega(\xi_{o})\,\xi_{so} + \alpha\,(\theta - \theta_{o}). \tag{3.4}$$

The SMA elastic modulus $D(\varepsilon, \xi, \theta)$ has been assumed linear with martensite volume fraction by many researchers,

$$D(\xi) = D_{a} + \xi\,(D_{m} - D_{a}). \tag{3.5}$$

However, since the proposed procedure is originally nonlinear, it can accommodate any nonlinear relations for the SMA modulus of elasticity that might exist in literature.

The SMA transformation tensor was assumed to be a function of the SMA modulus of elasticity by Brinson (1993) and is given as,

$$\Omega(\xi) = -\varepsilon_L D(\xi) . \tag{3.6}$$

It was also suggested that the term related to the coefficient of thermal expansion of the SMA, α, be considered constant due to its small value compared the modulus of elasticity of the material. Though, as it will be shown in the derivation of the electro-thermal SMA procedure in the subsequent section, the present procedure can incorporate this term as a function of other variables, such as the martensite volume fraction.

Using the above expressions, the term ${}^{t}C_{ijrs}$ could be derived. The derivation procedure is given in Appendix A2, which ultimately gives:

$$\frac{\partial \sigma}{\partial \varepsilon} = \frac{1}{\left[1-(D_m - D_a)\frac{\partial \xi}{\partial \sigma}(\varepsilon+1) + \frac{\partial \xi_s}{\partial \sigma}\right]} D(\xi) , \tag{3.7}$$

which could be represented as:

$$\frac{\partial \sigma}{\partial \varepsilon} = \frac{1}{\beta} D(\xi) , \tag{3.8}$$

$$\text{where, } \beta = \begin{bmatrix} 1 & \frac{\partial \xi_s}{\partial \sigma} & \frac{\partial \xi}{\partial \sigma} \end{bmatrix} \begin{bmatrix} 1 \\ 1 \\ -(D_m - D_a)(\varepsilon+1) \end{bmatrix} . \tag{3.9}$$

In order to determine $\frac{\partial \sigma}{\partial \varepsilon}$, derivations of the martensite volume fraction with respect to the stress of the SMA element at any time step, $\left[\frac{\partial \xi}{\partial \sigma} \; \frac{\partial \xi_s}{\partial \sigma} \right]$, need to be determined first. Kinetic relations presented in the above Brinson (1993) model are used for that purpose; the relations are differentiated with respect to stress to give the required derivative at any time step. Example of derivation of the kinetic relations for a SMA element transforming to detwinned martensite is given by:

$$\frac{\partial \xi_s}{\partial \sigma} = -\frac{\pi}{\sigma_s^{cr} - \sigma_f^{cr}} \frac{1 - \xi_{so}}{2} \sin\left\{ \frac{\pi}{\sigma_s^{cr} - \sigma_f^{cr}} [\sigma - \sigma_f^{cr} - C_M(\theta - M_s)] \right\}, \tag{3.10}$$

$$\frac{\partial \xi_\theta}{\partial \sigma} = -\frac{\xi_{\theta o}}{1 - \xi_{so}} \frac{\partial \xi_s}{\partial \varepsilon}, \tag{3.11}$$

$$\frac{\partial \xi}{\partial \varepsilon} = \frac{\partial \xi_s}{\partial \varepsilon} + \frac{\partial \xi_\theta}{\partial \varepsilon} = \left(1 - \frac{\xi_{\theta o}}{1 - \xi_{so}} \right) \left(-\frac{\pi}{\sigma_s^{cr} - \sigma_f^{cr}} \frac{1 - \xi_{so}}{2} \sin\left\{ \frac{\pi}{\sigma_s^{cr} - \sigma_f^{cr}} [\sigma - \sigma_f^{cr} - C_M(\theta - M_s)] \right\} \right)$$

...(3.12)

Note that nodes subscripts indicate initial conditions. Derivation of the above expressions for an SMA element transforming to detwinned martensite below the martensite start temperature and transforming to austenite are given in Appendix A3.

Equations (3.10)-(3.12) should be evaluated according to the phase of the alloy at current time step; they should be re-evaluated at subsequent time steps then substituted in

Equation (2.9) in order to get ${}^{t}C_{ijrs}$, which is then used to find the linear portion of the stiffness matrix for each SMA element at each time step.

It is worthwhile to note here that not only the SMA elements configurations are evaluated at each time step, but due to large deformations assumption, the linear and nonlinear strain-deformation matrices, ${}^{t}B_{L}$ and ${}^{t}B_{NL}$, will be dependent on the system deformation, and therefore they need to be evaluated at each time step as well. Also, it is worthwhile to note that this procedure can accept a wide variety of SMA constitutive models. One procedure is used here to illustrate the procedure.

3.2 SMA Finite Element Thermo-Electrical Frame Work

Since most SMA components used in smart systems are actuated electro-thermally, and recalling the fact that the temperature of a SMA has a significant effect on the phase transformation process (Leo et al 1994), the need for a transient nonlinear electro-thermal FE procedure for these applications arises. In this case the nonlinearity is due to the dependency of the material properties on the martensite volume fraction, which is dependent on the stress and temperature configurations of the system. Therefore, the SMA elements' thermal properties are dependent, although indirectly, on the temperature and stress configurations of the system which leads to the nonlinearity in the thermal system. Note that the structural and the thermal procedures are coupled. Based on the above, the derivation of the SMA nonlinear electro-thermal finite element proceeds as follow.

The general transient nonlinear heat transfer relation in variational form, , is given by (Bathe, 1996):

$$\int_V \delta\theta^T\, {}^{t+\Delta t}(\rho c)\, \dot{\theta}\, d^nV + \int_V \delta\theta^T\, {}^{t+\Delta t}k\, {}^{t+\Delta t}\theta\, d^nV = {}^{t+\Delta t}\Im + \int_S \delta\theta^S\, {}^{t+\Delta t}h({}^{t+\Delta t}\theta_e - {}^{t+\Delta t}\theta^S)\, dS_c + \int_S \delta\theta^S\, {}^{t+\Delta t}\kappa({}^{t+\Delta t}\theta_r - {}^{t+\Delta t}\theta^S)\, dS_r \quad , \qquad \ldots. (3.13)$$

Finite element discretization of the above relation gives,

$${}^{t+\Delta t}C^{(i)}\ {}^{t+\Delta t}\dot{\theta}^{(i)} + ({}^{t+\Delta t}K^{k(i-1)} + {}^{t+\Delta t}K^{c(i-1)})\,\Delta\theta^{(i)} = {}^{t+\Delta t}Q^{(i-1)} + {}^{t+\Delta t}Q^{c(i-1)} - {}^{t+\Delta t}Q^{k(i-1)}, \qquad (3.14)$$

where,

$${}^{t+\Delta t}\theta^{(i)} = {}^{t+\Delta t}\theta^{(i-1)} + \Delta\theta^{(i)}. \qquad (3.15)$$

The expressions for the above variables for m number of elements are given in Appendix A3. Using an Euler backward method for implicit time integration (see Appendix A3), and recalling Newton-Raphson method for iteration at each step results in,

$$\left({}^{t+\Delta t}K^{(i-1)} + \frac{1}{\Delta t}\,{}^{t+\Delta t}C^{(i-1)}\right)\Delta\theta^{(i)} = {}^{t+\Delta t}\tilde{Q}^{(i-1)} - {}^{t+\Delta t}C^{(i-1)}\ {}^{t+\Delta t}\dot{\theta}^{(i-1)}, \qquad (3.16)$$

the electrical heating power, P, is included in ${}^{t+\Delta t}\tilde{Q}^{(i-1)}$ as:

$${}^{t+\Delta t}P = j^2\, {}^{t+\Delta t}\rho(\xi). \qquad (3.17)$$

System temperature and stress configurations will affect the resistivity,ρ, of the SMA element, which is assumed to be a function of the martensite volume fraction is taken in this work as follow:

$${}^{t+\Delta t}\rho(\xi) = \rho_a - {}^{t+\Delta t}\xi(\rho_a - \rho_m). \qquad (3.18)$$

The heat generated due to latent heat evolved during SMA element phase transformations must be included in the heat generation expression. The following expressions are used to account for the latent heat and the electrical heating effects:

$$ {}^{t+\Delta t}Q^{(i-1)} = \sum_{m} \int_{V^{(m)}} H^{(m)T} \; {}^{t+\Delta t}Q_l^{m(i-1)} \, d^oV + \sum_{m} \int_{V^{(m)}} H^{(m)T} \; {}^{t+\Delta t}P^{m(i-1)} \, dV \quad , \tag{3.19} $$

where $ {}^{t+\Delta t}Q_l = q\dot{\xi} $, (3.20)

and by using implicit time integration $ \dot{\xi} = \frac{\partial \xi}{\partial t} = \frac{{}^{t+\Delta t}\xi - {}^{t}\xi}{\Delta t} $. (3.21)

3.3 Solution Procedure

Although the structural and the electro-thermal finite element procedures have been derived separately, they are actually coupled. The source of coupling between these two fields is the martensite volume fraction, which is dependent on the stress and the temperature configurations of the system. All SMA properties will be dependent on the stress and the temperature configurations of the system.

The solution procedure is dependant mainly on calculating the martensite volume fraction. An iterative solution using the Newton-Raphson method is used to minimize the errors due to linearization of the structural and the electro-thermal procedures of the system.

The main advantage of the proposed procedure structure, Figure 3.1, is that it is formed of a group of modules each performing certain tasks in the procedure (e.g. kinetic relations module, constitutive model module,..etc.). This adds flexibility to the procedure to accommodate any model simply by replacing any of the modules by another one without affecting the overall procedure (e.g. replacing the kinematics' relation module with the appropriate one according to the geometry of the application).

The procedure's sequence is summarized as follow:

1) Using the configurations at time zero, the stiffness matrices are evaluated.
2) The stiffness matrices and the corresponding force vectors are then used to evaluate the displacement vector.
3) Strains at the nodes are evaluated using the displacements of the nodes obtained from the previous step, and the kinematics relations (which may vary according to the geometry of the system).
4) Estimation of the stress configuration of the system is now calculated based on the strains of the nodes and using the system constitutive relations.
5) Then, or in parallel to that (while parallel computing is available), the electro-thermal module is fed with the initial martensite volume fraction and the electro-thermal loading configuration of the current time step, to obtain estimation of the temperature configuration of the system.
6) Both the stress and the temperature configuration estimates obtained in steps 4 and 5 are then fed to the kinetics of transformation relations for a better estimate of the martensite volume fraction configuration of SMA elements in the system.
7) Steps 1 to 6 are repeated again until a certain tolerance in the estimation of the martensite volume fraction in two subsequent iterations is reached.
8) Due to the linearization of the system, further iteration should be done by taking the resulting stresses and temperatures from the previous iterative solution and use it to update the properties of the system and go through steps 1 to 7 in an iterative solution until convergence criterion is achieved, after which, the loads

are incremented according to the loading configuration in the following time step and the process is repeated again.

Different convergence criteria could be utilized in this procedure. We found that the one based on minimization of the out of balance force is the most effective from the point of view of number of iterations needed to reach minimum error. The minimization of the out of balance forces criterion is given in Appendix A7.

3.4 Validation of the Numerical Results and Discussion

Validation of the model was performed by simulating experimental and numerical cases that have been introduced in the literature; the results were then compared to those obtained using the current procedure. The main objective was to show that the proposed procedure is capable of simulating coupled field SMA systems taking into consideration variable material properties of the SMA, and also to demonstrate the capability of the procedure to model the pseudoelasticity and the shape memory effects of the SMA, and consequently, show the capability of the proposed procedure to simulate SMA components used in smart systems.

The validation was done on three stages as follow:

(1) Validation of the electro-thermal procedure with variable properties.

(2) Validation of the thermo-structural procedure with variable properties

(3) Validation of the shape memory effect.

The three validation cases are explained in the following subsections.

3.4.1 Validation of the electro-thermal procedure with variable material properties

This was done by considering the problem solved by Amalraj et al (1999), where they numerically modeled the temperature distribution in a SMA wire with variable material properties that undergoes transformation from martensite to austenite. The transformation was purely thermally induced. The studied model accounted for the evolution in thermal conductivity, electrical resistivity and heat capacity, and it considered joule heating effects and heat transfer by convection along the surface of the wire. At the end of the wire three different boundary conditions were considered, they are convection, isothermal and adiabatic boundary conditions. Each proved to have a completely different effect on the temperature distribution along the wire.

The problem with the three different boundary conditions was modeled and solved using the proposed procedure. In order to minimize modeling errors, we used the same material properties (see Table.2) with variable SMA material properties (see Appendix A6 for SMA material functions used). Also, the same SMA kinetic model that was used by Amalraj et al was used in our model, although it is different from the one used as an example in section 2 in this paper (see Appendix A5). This demonstrated the flexibility of the proposed procedure to accommodate a variety of SMA constitutive and kinetic relations with variable boundary conditions, unlike the FEM procedure that was used by Amalraj et al for solving the same problem, which is understandably restricted to solving the proposed problem using specific kinetic relations.

The comparison of the results for the temperature distribution along the SMA wire for the adiabatic, convection and isothermal boundary conditions at the end are

shown in Figure.2. The temperature distribution results were captured after 10 seconds of heating by joule effect. The results show very good agreement between the proposed procedure and numerical procedure of Amalraj et al.

3.4.2 Validation of the thermo-structural procedure with variable material properties

Leo et al (1993) presented experimental results of a displacement-controlled elongation of SMA wire. In their study, they performed stress-strain experimental tests under different strain rates while having convection in air. The results showed that the hysteretic stress-strain curves depend strongly on the strain rates at which the wire is extended.

Their experiments were simulated using the current procedure for convection in air and in water at three different strain rates. We used the same material properties of the alloy they used in their experiments (Table.2). The SMA material functions used in modeling are given in Appendix A6. It was observed that strain rates mainly affect the rate of transformation and therefore affects the martensite volume fraction rate. This affects the evolution of latent heat, which increases the temperature of the wire at higher rates.

The comparison between the in-air experimental results by Leo et al and the finite element results are shown if Figures 3.3 , 3.4 and 3.5 for three different strain rates. The results show good agreement for the lower strain rates. At the highest strain rate, 6.4e-3 s^{-1}, the model estimates lower temperatures than the experimental results. We believe that this is due to the effect of heat generated due to deformation, which is not

taken into consideration in the current procedure. Also, one of the reasons for this shift, may be because the transformation interface is not moving as fast as the rate of deformation in this case, which might be the reason that led to the shift in the results in addition to the residual strain due to having residual martensite remaining at the end of the unloading process, which is noticed in the experimental results, Figure 3.5.

Therefore, it might be useful to consider a model that accounts for heat generation due to deformation or for the speed of motion of the transformation interface in the case of modeling high strain rate applications.

3.4.3 Validation of the shape memory effect with variable material properties

Liang et al (1990) presented stress-strain testing of a SMA wire, which is kept isothermally under the martensite start temperature. By loading the SMA wire, phase transformation takes place mainly by transforming from the twinned temperature induced martensite to the detwinned stress induced martensite which represents 100% of the martensite type by the end of the transformation process, which adds phase transformation strain to the wire extra to the mechanical stress-induced strain. By unloading the wire at the same temperature, the detwinned martensite remains stable, leading to an extended wire with zero stress.

The loading/unloading experiment was modeled using the current procedure using the same material properties of the alloy under experiment (Table.1) and assuming variable material properties. The experimental and the finite element results are compared in Figure.6. The data shows good agreement along the curve until the end of transformation,

after which, loading and unloading of the SMA wire result in a small hysteretic loop that couldn't be captured by the proposed model.

By reviewing the literature for the same problem, it was found that to date no numerical model seems to capture this hysteretic loop. We believe that this is a deficiency in the partcular SMA constitutive model used.

3.5 Concluding Remarks and Summary of the FEM Procedure

We have introduced a procedure for modeling SMA components subjected to a coupled structural and electro-thermal loading and having variable material properties. The solution of the proposed problem was reached by coupling nonlinear structural and nonlinear transient electro-thermal procedures through the martensite volume fraction of the SMA.

The main characteristics of the proposed procedure are its suitability for modeling multiphysics applications (e.g. subjected to electro-thermo-structural loading and boundary conditions) that incorporate SMA components, and its ability to accommodate variable SMA constitutive and kinetic models without being restricted to certain model. Most importantly, is its ability to accept any nonlinearity whether it is due to large deformations or due to SMA material functions (e.g. can accept SMA young's modulus even if it is function in temperature, stress and martensite volume fraction).

Also, and since its structure depends on modules, the proposed procedure can be extended to simulate 2-D and 3-D problems and different geometries (i.e. by using the appropriate kinematics relations), and can be linked to commercial finite element packages to add to it the feature of modeling SMA problems.

The procedure was validated by comparing experimental and numerical results obtained from literature with results of the finite element procedure. The validation showed that the proposed procedure is reliable for modeling the behavior of SMA due to multi-field loading, and in modeling the pseudoelasticity and shape memory behavior of the SMA. The proposed procedure is believed to be an effective tool for modeling SMA applications.

Table 3.1: SMA properties for different numerical & experimental verification problems.

Property	Unit	Leo et al 1993	Liang 1990	Amalraj et al 1999
Cross Sectional Area	mm^2	0.3339	Arbitrary*	0.0127
Length	mm	130	Arbitrary	40
Modulus of Elasticity (D_A)	GPa	69	67	Arbitrary
Modulus of Elasticity (D_M)	GPa	30	26.3	Arbitrary
Density	Kg/m^3	6450	6448.1	Arbitrary
M_F	K	282	282	322
M_S	K	292	291.4	332
A_S	K	310	307.5	345
A_F	K	322	322	355
S_{cr}^{S}	MPa	Arbitrary	100	Arbitrary
S_{cr}^{F}	MPa	Arbitrary	170	Arbitrary
Max. Shape memory strain (ε_L)	N/A**	0.068	0.067	Arbitrary
Latent Heat	$J\,mm^{-3}$	43×10^{-3}	Arbitrary	0.156
Electrical Resistivity (Rm)	$\Omega.mm$	Arbitrary	Arbitrary	6.993×10^{-4}
Electrical Resistivity (Ra)	$\Omega.mm$	Arbitrary	Arbitrary	8.693×10^{-4}
Heat Capacity (C_M)	$J\,mm^{-3}\,K^{-1}$	3.225×10^{-3}	Arbitrary	4.861×10^{-3}
Heat Capacity (C_A)	$J\,mm^{-3}\,K^{-1}$	5.401×10^{-3}	Arbitrary	5.401×10^{-3}
Thermal Conductivity (k_M)	$J\,mm^{-1}\,s^{-1}\,K^{-1}$	1.9×10^{-3}	Arbitrary	1.8×10^{-3}
Thermal Conductivity (k_A)	$J\,mm^{-1}\,s^{-1}\,K^{-1}$	0.02	Arbitrary	1.8×10^{-2}
Convection Coefficient	$W\,mm^{-2}\,K^{-1}$	6.5×10^{-6}	Arbitrary	1.4×10^{-4}
Ambient Temperature	K	300	263	300
$S_{M \longrightarrow A}$	N/A	Arbitrary	Arbitrary	1.5

* Arbitrary = the value of this property wouldn't affect the results. ** N/A = the property is unitless.

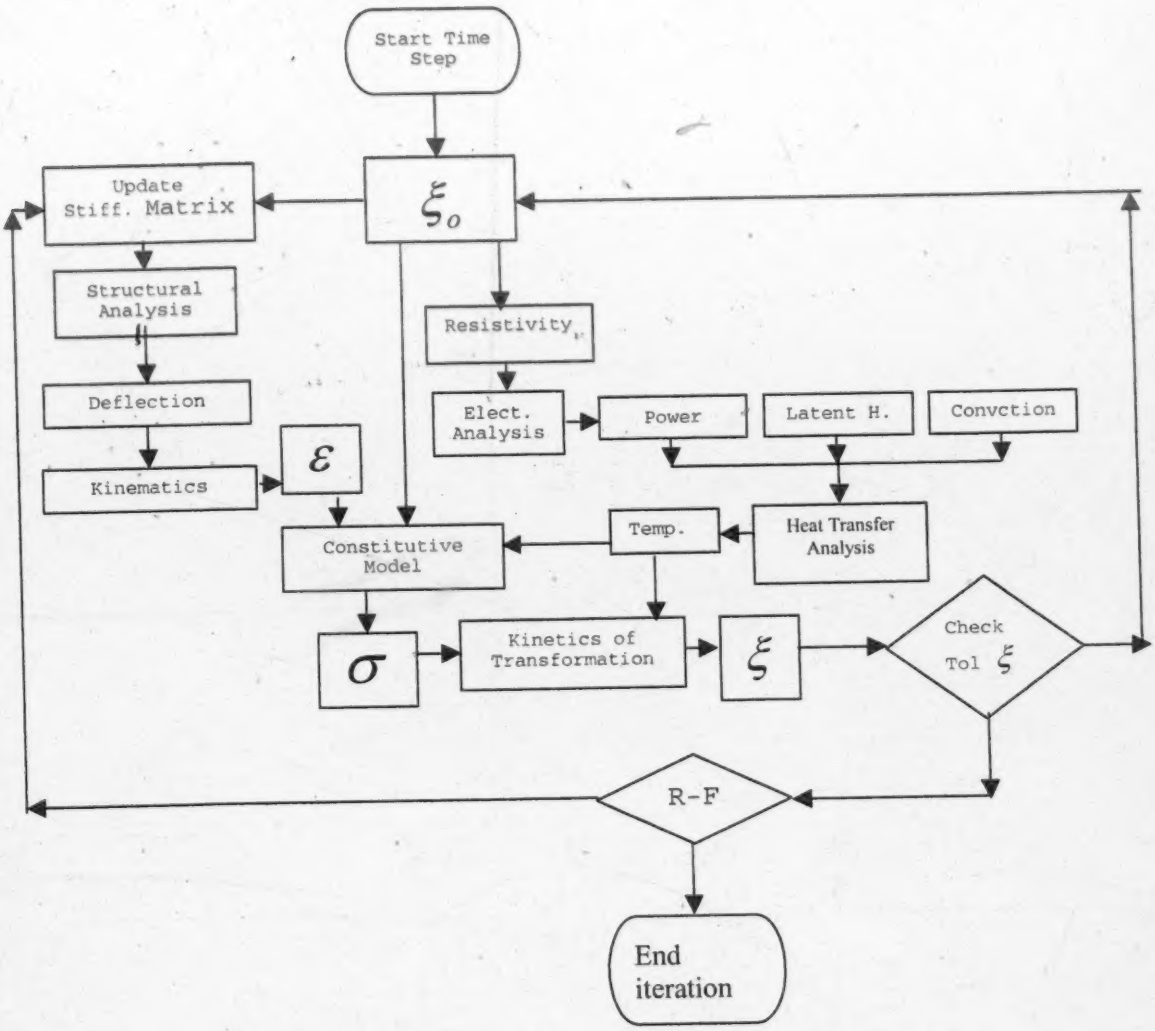

Figure 3.1: Nonlinear Coupled field solution procedure.

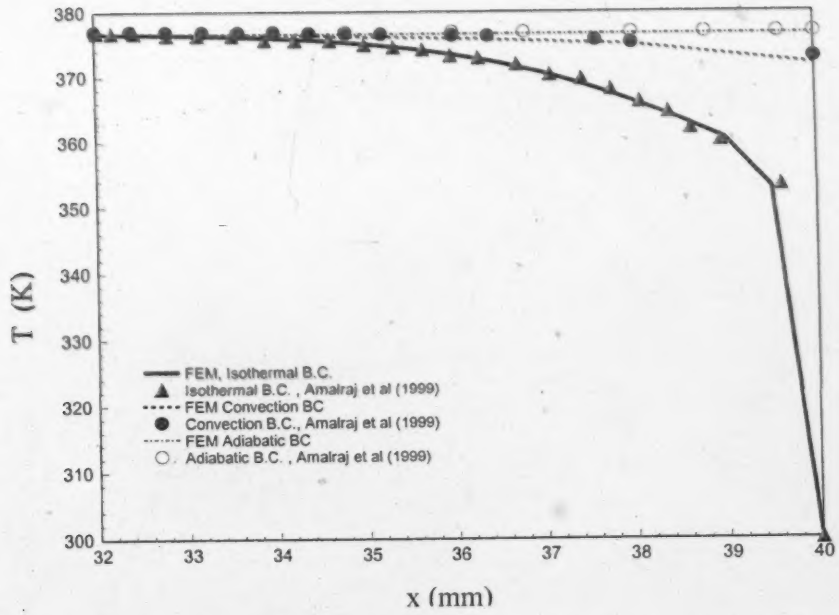
T (K)
x (mm)
FEM, Isothermal B.C.
Isothermal B.C. , Amalraj et al (1999)
FEM Convection BC
Convection B.C., Amalraj et al (1999)
FEM Adiabatic BC
Adiabatic B.C. , Amalraj et al (1999)

Figure 3.2: Temperature distribution along SMA wire after 10 sec., applying Convection, Isothermal and Adiabatic boundary conditions at the end.

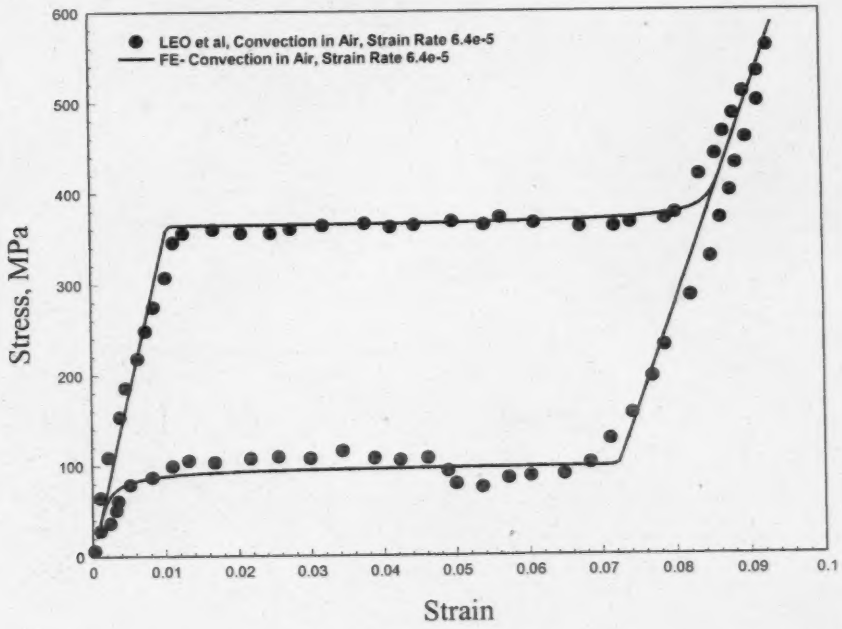

Figure 3.3: Stress –strain curve obtained by loading SMA wire at strain rate of 6.4e-5 and convection in air.

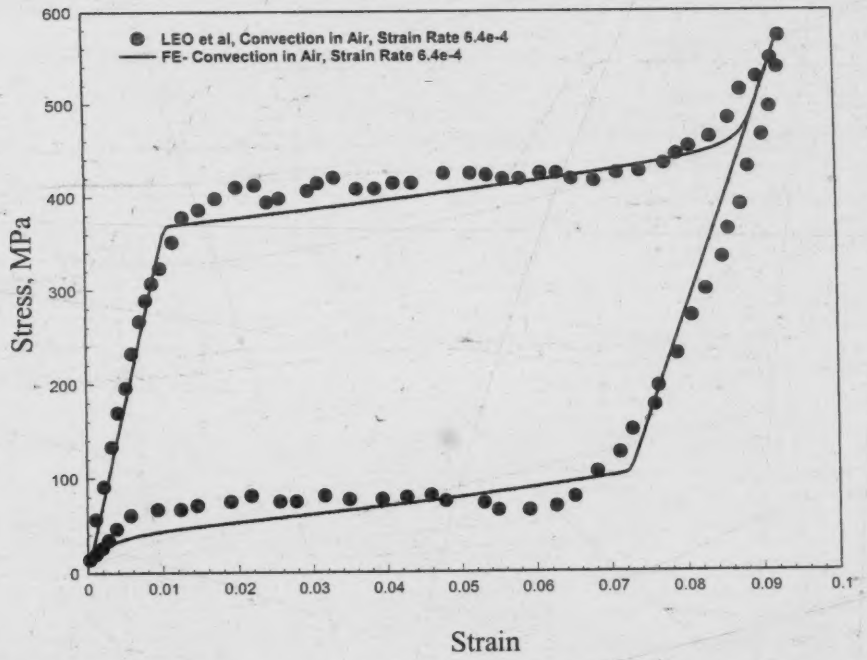

Figure 3.4: Stress –strain curve obtained by loading SMA wire at strain rate of 6.4e-4 and convection in air.

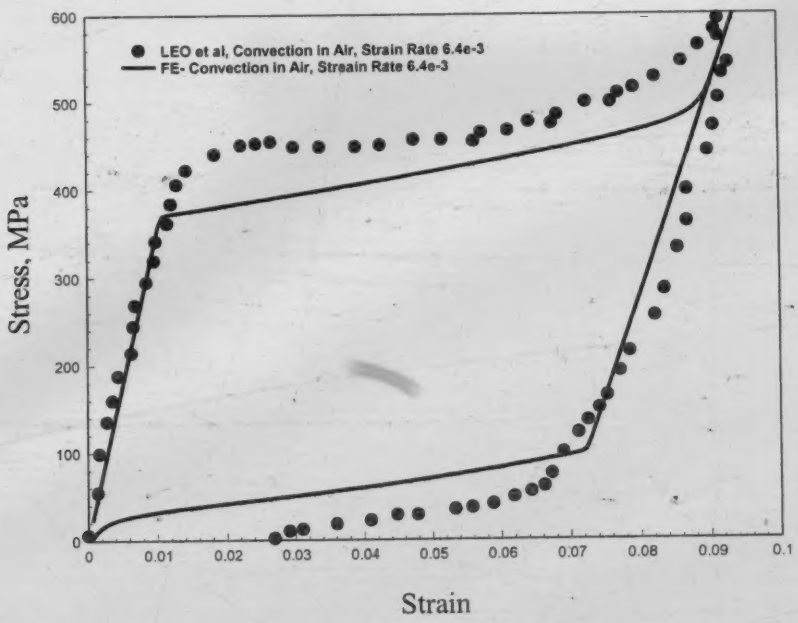

Figure 3.5: Stress –strain curve obtained by loading SMA wire at strain rate of 6.4e-3 and convection in air.

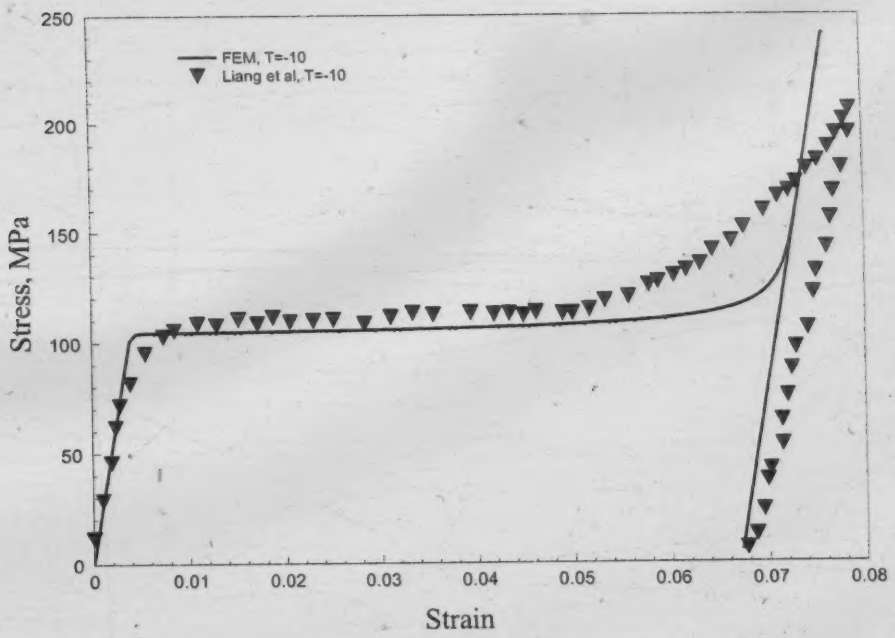

Figure 3.6: Stress –strain curve obtained by loading SMA at T=263 K (Below martensite start temperature).

4. FE analysis of the behavior of an SMA self-damage-control Smart System

In this chapter we utilize the FE procedure presented in Chapter 3 to investigate the behavior of SMA self-damage-control composite and to study the effect of changing various system parameters on its performance.

4.1 SMA Smart System's Simulation and Development

The proposed system (Figures 4.1 and 4.2) consists of SMA wires embedded in polymeric matrix. When the system is initially loaded during operation, and assuming no cracks or air inclusions in the matrix, both the matrix and the wires will be under uniform stresses and therefore uniform deformation. A crack generated at any spot in the polymeric matrix will result in increase in the elongation of the wires at this spot compared to elongation of the rest of the wires embedded in the matrix. This increase in elongation will consequently result in a change in the kinetic configurations of the SMA wire at the crack spot (i.e. martensite volume fraction of the wires due to stress at this spot will change), which will lead to change in the resistivity of the wire or group of wires affected by the crack elongation. The change in resistivity could be sensed through the affected wires by the means of an amplified electrical signal.

Analysis of the produced signal can give information about the place and the size of the opening of the crack, which is consequently further analyzed to estimate the amount of current required to actuate the affected wires based on the objective function of minimizing the crack tip stress intensity factor in order to minimize the probability of failure. After estimating the required current, a signal is generated by the system analyzer

and transferred to the SMA embedded wires through a signal amplifier to actuate the wires back to their original shape. This system achieves continuous monitoring of the structure and can minimize the risks of failure due to stress concentration at crack tips.

One of the potential applications of this system can be utilizing it for continuous monitoring and temporary repair of the bond between repair patches and aircraft skins. The SMA embedded- composite can be used as a smart-bond attaching repair patches to the aircraft skin where damage is most likely, Figure 4.3. As the bond is cracked due to high vibrations, the crack will be sensed and controlled by the system to minimize sudden failure of the skin at the spot of the crack. This system will be a useful tool as a continuous monitoring and first aid system in order to minimize the probability of failure of the aircraft skin due to failure of the bond between the repair patches and the skin.

The objective of the simulation process of the system is estimating the effect of different system variables on the actuation of the wires and on the stress intensity factor of a generated crack in order to characterize the performance of the smart system. Also, the results of the simulation could be used to develop a Neural Network based on the objective function of minimizing the stress intensity factor of the generated crack. This network can be used by the system analyzer to estimate the actuation signal for various cases. The application of the Neural Networks and the estimation of the system objective function is out of the scope of this work, although this could be done in future work.

4.2. Modeling and Assumptions

Modeling of the proposed system will require understanding of the sensing/actuating mechanism of SMA, modeling the smart composite components (i.e.

SMA wires and the polymeric matrix) and background of the crack-tip stress intensity factor parameter, which all will be discussed in the following subsections.

4.2.1 SMA Wires Sensing/Actuating Mechanisms

SMA's unique shape memory effect property is the fundamental property utilized in this application. If an SMA wire, initially at zero stresses and 100% austenite (see State(1) in Figure 4.4 and Table 4.3), was loaded to increase its stress at relatively constant temperature, partial transformation of the austenite to detwinned martensite would take place, State (2) in Figure 4.4. Detwinned martensite is characterized by distortion in the crystal structure, which leads to deformation of the SMA wire. If a partially austenite / partially detwinned martensite wire is unloaded at a temperature lower than the austenite start temperature, the detwinned martensite remains stable and won't transform back to twinned martensite resulting in a deformed wire, State (3) in Figure 4.4.

The detwinned martensite can remain stable up to a temperature below the austenite start temperature. At this temperature, the detwinned martensite phase is not stable and a martensite crystal will start to transform to the austenite parent crystal. Therefore, if a partially austenite/ partially detwinned wire is initially at the austenite start temperature, the wire's phase will be sensitive to any increase in its temperature or stress.

The change in wire's phase could be utilized for both sensing and actuating purposes. For sensing, as the crack opens and percentage elongation of wire increases, tensile stresses increase in the wire, and therefore, the martensite volume fraction of that wire changes. Resistivity of the wire could be transformed to percentage elongation in the wire by using the wire's resistivity-phase transformation and constitutive relations.

To actuate the wire, an increase in the wire temperature will lead to phase transformation of the wire from martensite phase to austenite phase leading to contraction of the wire, which is the main actuation direction required for this application.

4.2.2 SMA Nonlinear Structural Finite Element Derivation

In order to model the electro-thermo-mechanical behavior of shape memory alloy embedded wires with variable material properties, a nonlinear 1-D shape memory alloy finite element was developed first.

SMA wires embedded in the composite can be subjected to large elastic strain up to 8%. Therefore, a SMA 1-D finite element should take large deformations into consideration. The 1-D SMA structural element introduced in Section 3.1 is the element used here to mesh the SMA embedded wires for the structural analysis.

4.2.3 SMA Electro-thermal Finite Element Derivation

SMA embedded wires in the smart composite are going to be actuated electro-thermally. Recalling the fact that the temperature of a SMA has a significant effect on the phase transformation process (Leo et al 1994), SMA nonlinear electro-thermal element need to be used to model the electro-thermal behavior of the SMA embedded wires. The source of nonlinearity of the SMA electro-thermal element in this case is the dependency of the material properties on the martensite volume fraction which is dependent on the stress and temperature configurations of the system. Therefore, the SMA elements' thermal properties are dependent, although indirectly, on the temperature and stress configurations of the system which leads to nonlinearity of the thermal system as well.

The 1-D SMA nonlinear electro-thermal finite element introduced in Section 3.2 is the element used here to mesh the SMA embedded wires at the electro-thermal analysis.

4.2.4 Two-dimensional Thermo-structural Finite element Derivation

The matrix of the smart composite is assumed to be linear, elastic and isotropic. A linear two-dimensional element will be used to model such matrix. Due to the thermal effect of the heated SMA wires embedded in the matrix which will lead to thermal expansion of the matrix, thermo-structural effects must be considered in the composite-matrix element for which the thermal strain is given by:

$$\varepsilon_{11}^{th} = \alpha_r(\theta - \theta_o), \varepsilon_{22}^{th} = \alpha_r(\theta - \theta_o) \text{ and } \varepsilon_{33}^{th} = 0. \tag{4.1}$$

The total element stresses will be due to the total strains and thermal strains as follow (Bathe, 1996):

$$\sigma_{ij} = C_r(\varepsilon_{ij} - \varepsilon_{ij}^{th}). \tag{4.2}$$

For a plane stress thermo-structural element, this becomes

$$\sigma_{ij} = \frac{E\alpha_r}{1-\nu^2}\begin{bmatrix} 1 & \nu & 0 \\ \nu & 1 & 0 \\ 0 & 0 & \dfrac{1-\nu}{2} \end{bmatrix}\begin{bmatrix} 1 \\ 1 \\ 0 \end{bmatrix}\left\{\sum_{i=1}^{4}(H_{ri}\theta_{ri}) - \theta_o\right\}. \tag{4.3}$$

Note that, the subscripts 11,22,33 and ij are all indices of the strain and stress components.

4.2.5 Crack-tip stress intensity factor

The deformation of the crack is assumed to be in the elastic stage, therefore the concepts and assumptions of Linear Elastic Fracture Mechanics (LEFM), (Section 2.5),

are used to model the relation between the stresses at the surface of the crack and the crack tip stress intensity factor (refer to section 2.5 for formulation).

4.2.6 SMA Wires Material Properties Evolution Functions

The SMA material properties evolution functions of at any time, t, are assumed to be linear with the martensite volume fraction. For example the SMA elements' thermal conductivity evolution function is,

$$'k(\xi) = k_A - {}'\xi(k_A - k_M),$$

all other SMA properties including the coefficient of thermal expansion are assumed to have the same relation with the martensite volume fraction Appendix A6. This assumption has been taken by many authors in literature (e.g. Amalraj et al, 1999) and is believed to be acceptable for wide range of shape memory alloys.

4.3. Model Description and Solution Procedure

Figure 4.5 illustrates the FE meshed model and boundary conditions. In general, the FE model consists of 2-node-SMA wire elements with each of their nodes connected to one of the 4-node- matrix quad elements. The crack at the middle of the composite is simulated by having some unconnected and unconstrained matrix nodes. Convection between both surfaces of the composite and the surrounding air is assumed, and the external forces are modeled as uniform distributed loads at the top edge of the composite, Figure 4.1. Details about the meshing process, the sequence of modeling and the solution are stated in the following points:

1- SMA wires are initially meshed using the SMA nonlinear structural finite elements, and connected to the elements of the polymeric matrix, which is meshed using the thermo-structural 2-D elements with finer meshing at the crack edges.

2- The system is initially solved for structural deformation due to applied stresses. Then the SMA wires are re-meshed using the electro-thermal SMA finite elements, and the whole system is solved for temperatures at the nodes due to the current going through the SMA wires.

3- Temperatures at the nodes are used to solve for the deformation and stresses of the polymeric matrix nodes due to heat expansion and to estimate the phase of the SMA wire at this time step.

4- SMA wires are re-meshed again using the structural SMA elements and system configurations obtained from the previous step is used for structural solution of the whole system again.

5- The system is checked for convergence, using the out-of-balance load vector criterion (Appendix A7).

6- If convergence isn't attained, steps 3 and 4 are repeated and as convergence is reached, the crack tip stress intensity factor is calculated according to step.7 and the solution moves to the next time step configuration.

7- The SIF of the crack is calculated by exporting the nodes and elements with their current force configuration to ANSYS, where the SIF is calculated automatically using the ANSYS Fracture Mechanics Analysis.

4.4.Application and Discussion

4.4.1 Smart System Sensing/Actuating Response

The system's sensing/actuating response was studied first in order to understand the system properly.

Sensing Response. The sensing simulation was done by initiating a small crack and then applying external stresses to the smart composite without actuating the wires. As the external load increases the crack size increases and the SMA wires' extension at the crack increases. The stress intensity factor at the crack is calculated as the external stresses are increased and the corresponding change in the wire's martensite volume fraction is recorded. The relation between the wires' resistivity and wires' martensite volume fraction can be calculated using SMA wires evolution functions (refer to Section 4.2.6). The relation between the SMA wires' martensite volume fraction and the corresponding SIF of the crack is plotted Figure 4.6. It is noticed from the graph that the relation is linear. This figure can be used by the system analyzer as a calibration graph by transforming the sensed resistivity into the corresponding SIF of the crack at any time. This will achieve continuous monitoring of the a crack status.

Actuating Response. The SIF of the crack is now the input value to the *Actuating System,* which consists of the system analyzer and the electro-thermal actuating devices (Figure 4.1). According to the SIF of the system, the system analyzer will be able to estimate the appropriate current that should be applied to the SMA wires in order to recover the crack.

The actuation process is simulated by assuming a cracked smart composite under certain external stress, then applying different currents to the wires to actuate them, then recording the change in the SIF of the crack as the temperature of the wire rises. Figure 4.7 shows the relation between stress difference, ΔS, which is the difference between the current stress of the wires and their initial stress, and temperature difference, ΔT, which is difference between the temperature of the wires and their initial temperature. From the figure, it is noticed that the wires are initially under a considerably small negative stress difference (i.e. the tensile stresses in the wires decreases), and then as transformation starts these stresses increase and become positive. The reason for that is believed to be due to the differences in the Coefficient of Thermal Expansions (CTE) between the SMA wires and the polymeric matrix. Before transformation starts, SMA wires tends to expand more than the polymeric matrix leading to slightly small compressive stresses applied on the SMA wires from the matrix. As transformation starts, SMA wires tries to contract due to transformation forces, and at certain point, a balance occurs between the transformation forces and forces due to CTE difference, after which, the transformation forces become higher and reactions of the polymeric matrix on the wires change from compressive to tensile. Figure 4.8 shows a simulation of the crack tip shape as SMA wires are actuated. The crack tends to close as temperature increases (i.e. wires are actuated) and consequently SIF of the crack improves (become smaller).

4.4.2 Parametric Study

A parametric study was performed on the above-introduced model. The study was performed by fixing all the system parameters, Table 4.1, and varying a single

parameter at the time to study its effect on the performance of the system. The objective of this study is giving a clear illustration on the performance of the system and different parameters affecting it. The study is introduced in the following paragraphs.

Effect of Current Density. The investigation of the effect of the current density on the system's behavior is done by fixing all the properties of the system and actuating the wires at current densities ranging between 2 - 12 amp/mm^2. As shown in Figure 4.9, the density of the current running through the SMA wire mainly affects the time needed to reach the minimum crack stress intensity factor and to recover the crack. As the current increases, the heat power input increases leading to higher rate of temperature rise and faster phase transformation. The start of phase transformation in the wires could be detected in Figure 4.9, by noticing the sudden change in the slopes; this change indicates that higher forces of contraction are generated due to the phase transformation.

Figure 4.10, shows the effect of increasing the current density in the wires on the stress intensity factors at different times, it is clear from this figure that stress intensity factor is improving faster as the current density increases.

Selecting the appropriate current density is not only governed by the speed of the crack recovery. As mentioned above, increasing current density leads to increasing temperature rates which are directly proportional to the heat power, in other words, increasing the current density increases the heat power input to the system, which might cause harmful effects for certain systems. Figure 4.11 can be useful in this matter, if the highest permissible temperature increase rate of the system is known, and according to the SIF of the crack at certain moment, the above mentioned figure can be used by the

system analyzer to determine the maximum allowable current density that can be used to heal the crack.

On the other hand, the selected current densities shouldn't be lower than certain values (about 6 amp/ mm^2 in our case- refer to Figure 4.10) below which, applying current might have no effect on the recovery process as steady state heat transfer through the system is reached at temperatures lower than transformation temperatures and therefore not enough recovery forces are generated.

Effect of Wire Diameter Size. Different SMA wires of diameters 0.2, 0.3 and 0.4 mm were used in the system's simulation to investigate the effect of changing SMA wires' diameter on the system's performance. The wires are actuated at constant current of 0.25 amps (i.e. almost constant power). By increasing the SMA wires diameter, two main factors will be affected. First, the force generated by wire will increase due to the increase in the cross sectional area of the wires. Second, the surface area of the wires will increase, which is linearly related to heat power loss by conduction at the surfaces of the wires.

Therefore, by assuming constant power input, increasing wire diameter affects by increasing internal forces applied by wires due to stresses, and by increasing the heat loss by conduction at the surface of the wires. The resultant of the interaction of both effects is shown in Figure 4.12, which shows the effect of increasing wire diameter on the crack recovery process. It is noticed from the graph that the larger the SMA wire diameter, the longer the time is required until crack is recovered, and the higher the SIF of the crack before the transformation process (i.e. due to the difference in CTE effect).

Though, the graph shows that the increase in the SIF of the crack before transformation almost doesn't change when the diameter of the wires was increased from 0.3 to 0.4 mm while the crack recovery process was severely affected by this slight increase in diameter. From this we concluded that by increasing SMA wires' diameters, heat loss by conduction becomes the dominating effect on the crack recovery process.

Effect of Number of Actuated Wires. Figure 4.13 illustrates a schematic diagram of how the number of actuated wires per crack are increased. As the number of actuated wires per crack increases the summation of forces at the crack spot increases, and therefore, less force per SMA wire will be needed to recover the crack. As a result, less transformation is needed and consequently less recovery time.

Figures 4.14 and 4.15 shows the effect of increasing the number of actuated wires per crack on crack recovery process. From Figure 4.14 it is noticed that as the number of actuated wires increases, less time is needed to crack recovery. This fact is further illustrated in Figure 4.15, which indicates that as the number of wires increases less phase transformation per wire is required to recover the crack, hence, less time is needed. Figure 4.14 also shows that increasing number of wires per crack increases the SIF of the crack before transformation starts, which is due to the difference in CTE effect, though, this increase is noticed to be within 30% of the initial crack SIF.

Having larger number of wires can work favorably for sensitivity of system to small cracks and minimizes the risk of having undetected small cracks in between the wires. On the other hand, it should be noted that, increasing the number of wires changes

the composite composition, and consequently affects the global mechanical properties of the composite.

Effect of Applied stress. In order to study this effect on the system, externally applied stresses on the system were varied between 5 and 25 MPa.

Figures 4.17 and 4.18 shows the effect of increasing the externally applied stresses on the SIF of the system. As seen in Figure 4.17, increasing the externally applied stress increases the SIF of the crack linearly, and therefore, more SMA wires transformation forces are required. Therefore, more stress per wire is needed (Figure 4.17) as well as more phase transformation (Figure 4.18). Therefore in cases when large externally stresses are applied, higher current density or larger number of actuated wires might be needed to ensure generating enough recovery forces. On the other hand, increasing SMA wires' diameters should be avoided to avoid the above-mentioned difference in CTE effect, which might work with the high stress to fail the structure more rapidly.

Effect of SMA Wires' Prestrain. The study was performed by changing the SMA wires prestraining between 0.02 and 0.06 while keeping all the other system properties unchanged.

Figures.4.19 and 4.20, show that, unless it is too small (in this case <0.02) variation in the SMA wires' prestrain has a minor effect on the crack closing recovery process. This is further demonstrated in Figure 4.21, which shows that almost the same amount of transformation is needed per SMA wire to generate the required recovery

forces, and it seems that is amount is weakly related to the current phase of the SMA wire (which is determined by the amount of the prestrain in that wire).

On the other hand, If the SMA wires are not prestrained enough, the volume fraction of the detwinned martensite might not be enough to develop enough forces when totally recovered, leading to incomplete crack closing.

Effect of Heat Convection. In this study, heat convection coefficient between at the surfaces of the smart composite was varied between 1 x 10 –4 and 20 x 10 –4 watts/mm^{2}K while keeping all other system properties unchanged in order to study the effect of increasing heat dissipated by convection through the system.

Figures 4.22 and 4.23 show that as the heat dissipation increases, phase transformation takes place at slower rate. If the heat dissipation was high enough to reach steady state heat transfer, the rate of SMA wires' phase transformation would reach zero, and therefore phase transformation will stop. This might lead to incomplete crack recovery process, a case that should be avoided either by increasing the heat power input (through increasing the current density), decreasing the require transformation (through increasing the number of actuated wires per crack) or by decreasing heat dissipation by convection (by decreasing the heat convection coefficient if controllable).

Effect of System's Initial Temperature. This study was made by changing the initial temperature of wires and the initial and ambient temperature of the whole system between 278 and 303 K, while keeping all the other system properties unchanged. Note that the austenite start transformation temperature of the wires is at 310 K (Table 4.1).

The system's initial temperature mainly affects the time required until transformation starts as well as the maximum SIF of the crack. As the initial temperature gets closer to the austenite start temperature, the transformation process starts faster. But on the other hand, if the initial temperature was considerably lower than the austenite start temperature, more time is taken before transformation starts which might give chance to the system to reach steady state heat transfer before transformation temperature is reached or before enough transformation is attained.

Also, having longer time to transformation leads to increasing the harmful effect of the difference in CTE tensile forces, which is demonstrated in Figure 4.24 by the increase in SIF of the crack. This might lead eventually to failure of the system before recovery process really starts. This effect can only be avoided by controlling the initial temperature and making it closer the austenite start temperature as possible, or by selecting SMA wires with austenite start temperature close to the system's initial temperature.

Effect of Polymeric Matrix Material. This study was performed by considering different matrix (linear isotropic) materials while using the same SMA wires material and keeping all the system's other properties unchanged. A list of the tested matrix materials with their properties is given in Table 4.2.

Figure.4.25 shows the effect of varying the polymeric matrix material on the crack recovery process. It is noticed in this graph that material of almost the same modulus of elasticity tends to behave similarly, although their coefficients of thermal expansion are varying greatly. From this it is concluded that modulus of elasticity of the matrix material has more effects on the crack recovery process than its CTE. As shown in the above-mentioned figure, the higher the modulus of elasticity is, the faster the recovery process tends to be. This mainly because the higher the modulus of elasticity of the material the lower the SIF will be for the same crack. Figure 4.26 shows the martensite volume fraction rate of change with time for different matrix materials, from this figure it is noticed that matrix material's modulus of elasticity also have the main effect on the wire phase transformation process.

4.5 Concluding Remarks

The finite element procedure proposed in Chapter 3 was successfully used to model a smart-self –damage control system consisting SMA wires embedded in a polymeric matrix.

A parametric study was performed to investigate the effect of various parameters on the performance of the system. It was found that increasing current density speeds up the recovery process by adding more heat to the system. Also, it was found that by increasing wire diameters at constant power input, heat loss by conduction at the surface

of the wires becomes the dominant effect on the recovery process; therefore, more time is needed to recover the crack as the wires diameters are increased.

Increasing number of activated wires was found to be beneficial as it reduces the amount of phase transformation and forces required per wire, and increases system sensitivity to small cracks. It is suggested that convection coefficient not to be too low or to high, and the initial temperature of the system to be as close to the austenite start temperature as possible. It was found that modulus of elasticity of the matrix material has the major effect on the crack recovery process, and that SMA wires prestraining could have negligible effects if its not too low. The full conclusions are given in Chapter.5.

Table 4.1: Unchanged properties for various cases.

Property	Unit	Value
Geometrical Dimensions		
Wire Diameter	mm	0.2
Length	mm	10
Width	mm	10
Thickness	mm	0.5
Crack Width	mm	2
No. of Actuated wires / crack	mm	5
SMA Wires Properties		
Same as Liang et al SMA properties (refer Table 3.1)		
Polymeric Matrix Properties		
Elastic Modulus	GPa	2.5
CTE	mm/mm K	15×10^{-6}
Thermo-electrical Boundary Conditions		
Initial Temperature	K	303
Ambient Temperature	K	303
H.Convection Coeff.	Watt/mm^2 K	5×10^{-6}
Current Density	Amp/mm^2	8

Table 4.2: Different linear isotropic materials used for the effect of matrix material case study.

Material **	Modulus of Elasticity (GPa)	CTE (μm/mm K)
Material.1	11	21
Material.2	3	25
Material.3	2.5	15
Material.4	2.7	60
Material.5	20	14

** Materials 1 to 5 are different grades of the Epoxy polymer.

Table 4.3: Phases of different SMA wire states in Figure4.4.

State	Phase	Stress State	Temperature State
1	100% Austenite	Zero	Ms<T< As
2	Austenite- Detwinned Martensite mix.	> Zero	Ms<T< As
3	Detwinned M.+ Austenite mix	Arbitrary	< As
4	Detwinned M. partially transformed to Austenite	> Zero	> As

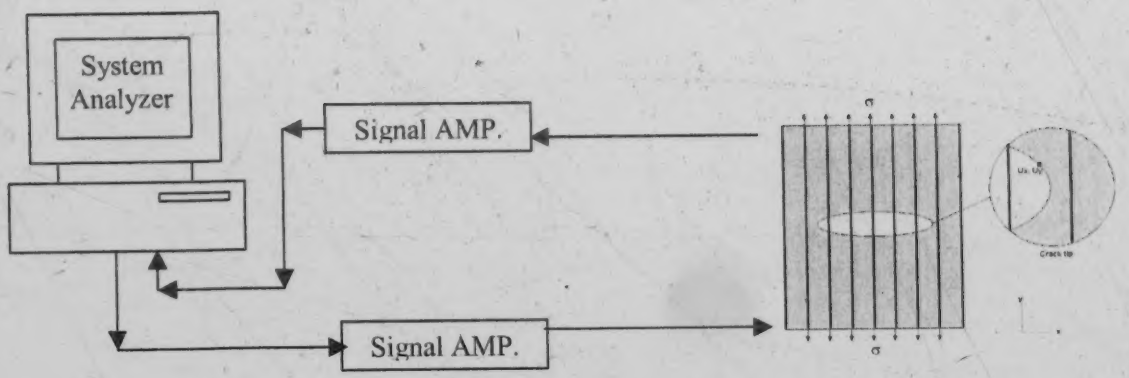

Figure 4.1: Crack Control Smart System.

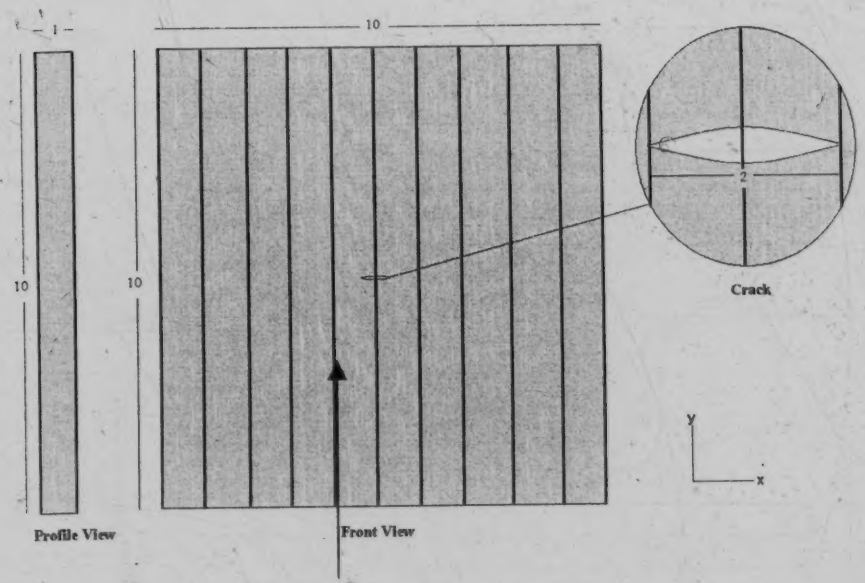

Figure 4.2: Profile, Front and Crack views of the model (dimensions in mm).

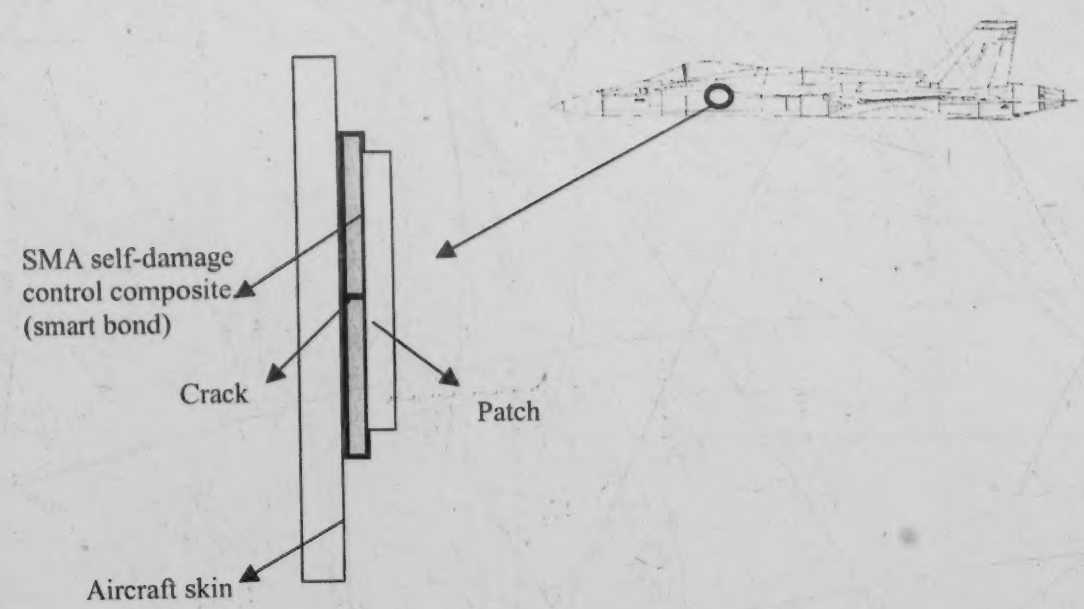

Figure 4.3: An SMA self damage control composite working as smart-bond between a patch and the aircraft skin.

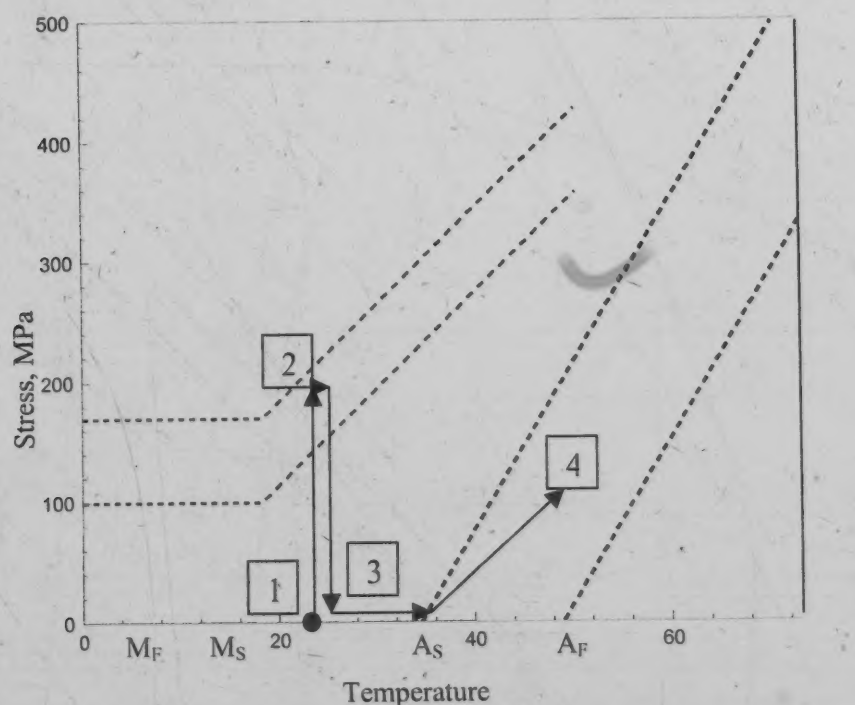

Figure 4.4: Schematic diagram of the SMA wires stress-temperature loading.

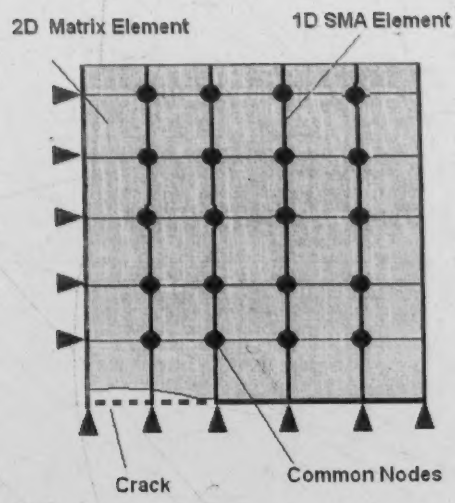

Figure 4.5: Schematic diagram of the system showing the constrained axes in the vertical and horizontal directions and the mesh.

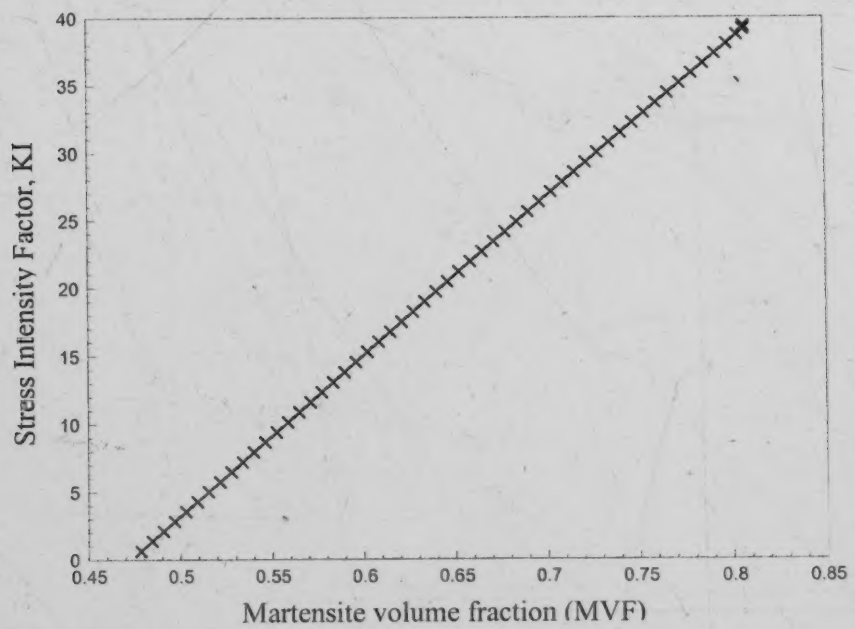

Figure 4.6: SMA martensite volume fraction versus SIF of the crack, for different cracks.

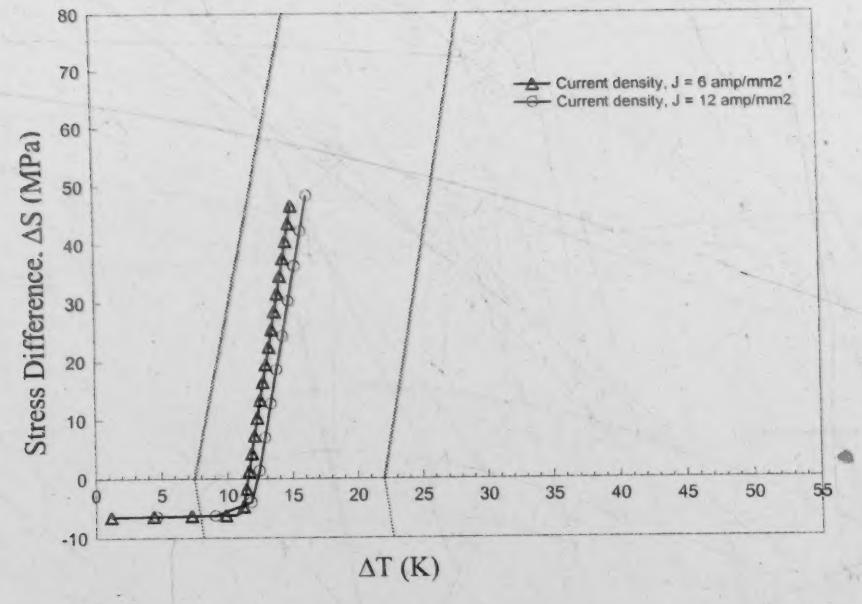

Figure 4.7: Typical SMA wires stress difference - temperature difference loading diagram.

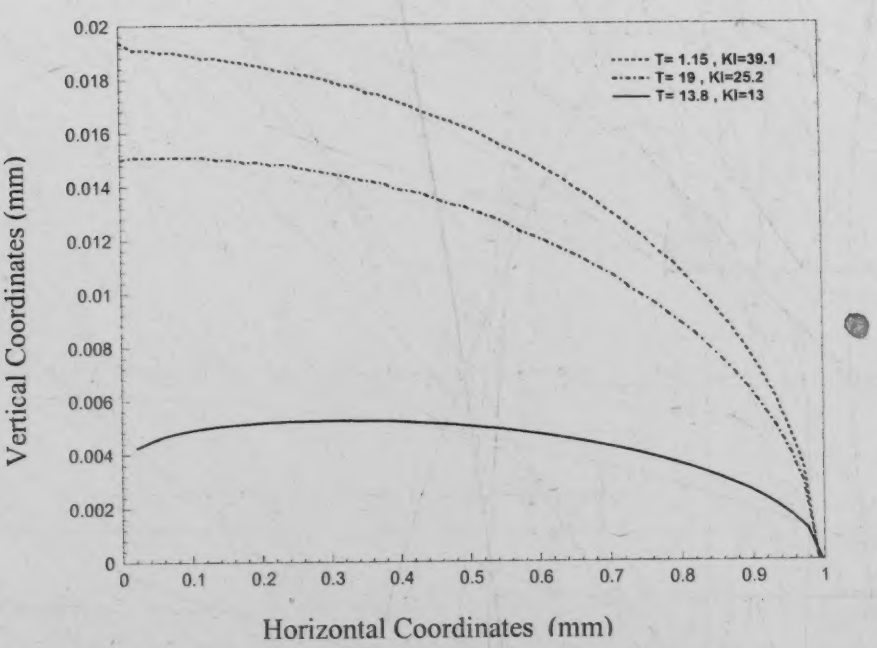

Figure 4.8: Crack tip shape at the different temperatures at Current density of 6 amp/mm^2.

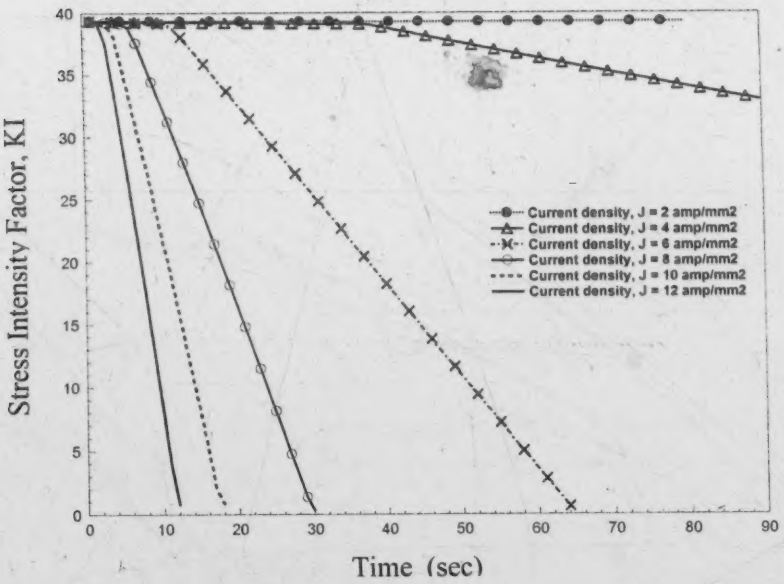
Stress Intensity Factor, KI
Time (sec)
Current density, J = 2 amp/mm2
Current density, J = 4 amp/mm2
Current density, J = 6 amp/mm2
Current density, J = 8 amp/mm2
Current density, J = 10 amp/mm2
Current density, J = 12 amp/mm2

Figure 4.9: Time versus stress intensity factor at different current densities.

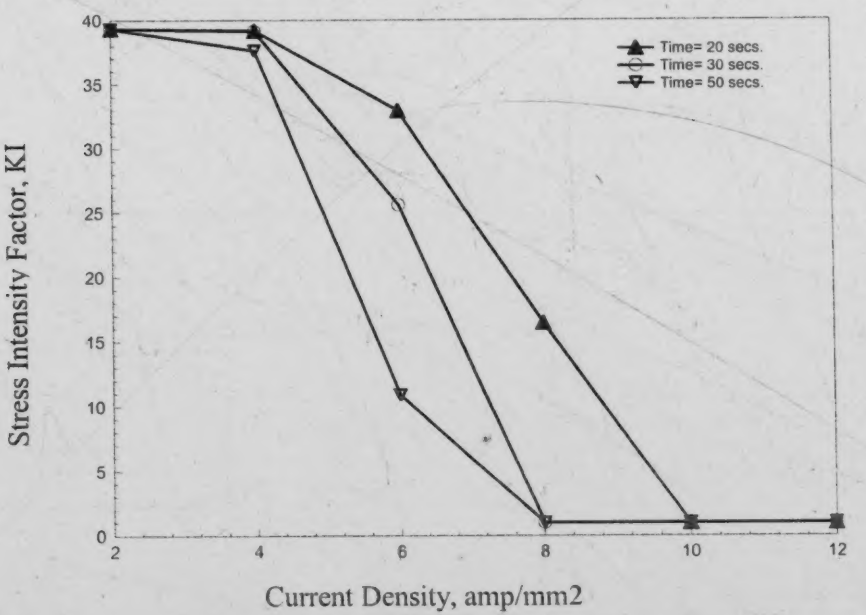

Figure 4.10: Effect of Increasing Current Density in the SMA wires on the SIF at different temperatures.

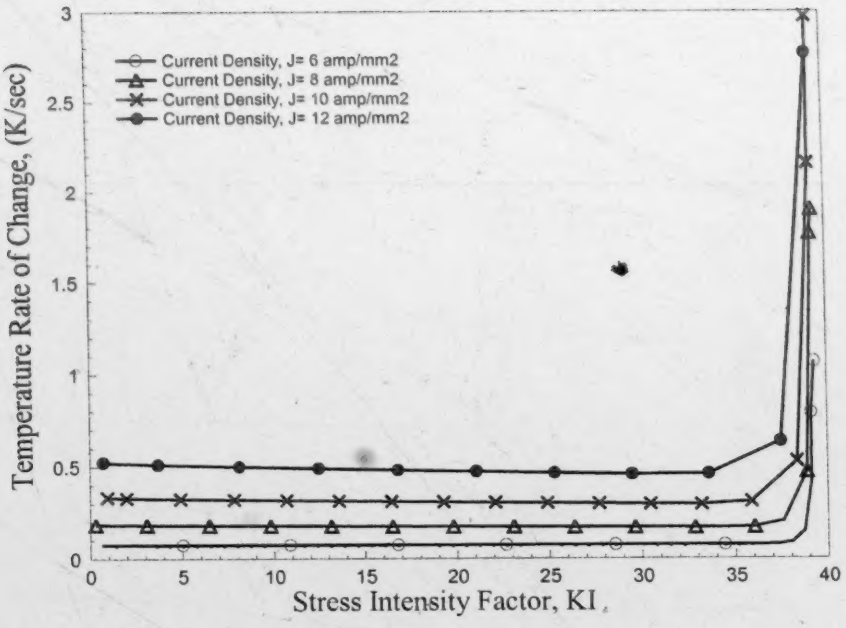

Figure 4.11: Rate of Temperature rise versus SIF at different current densities.

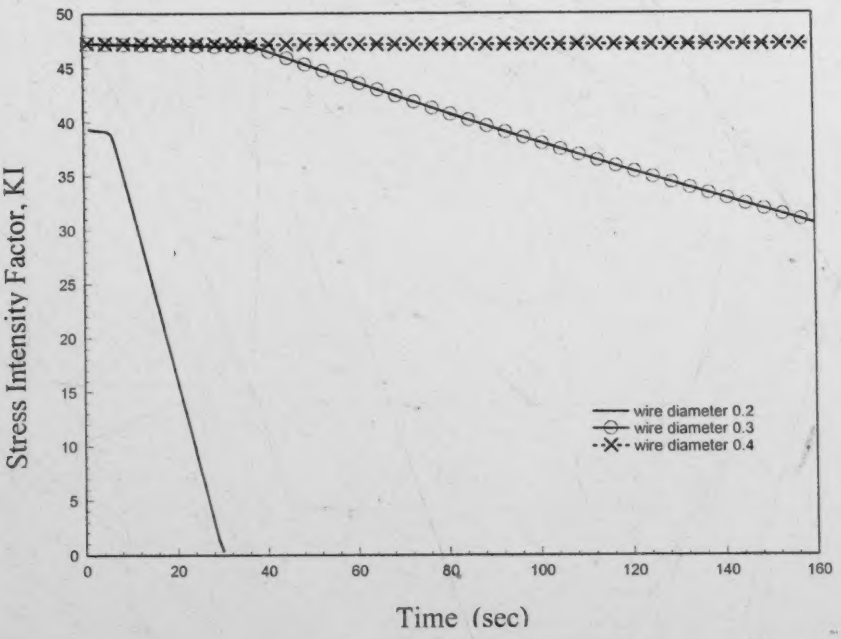

Figure 4.12: SIF of the crack versus Time at different wires' diameter, wires actuated at 0.25 amps.

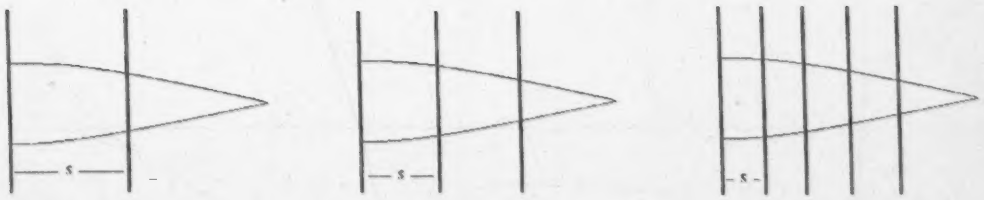

Figure 4.13: Schematic diagram of showing different number of actuated wires per crack.

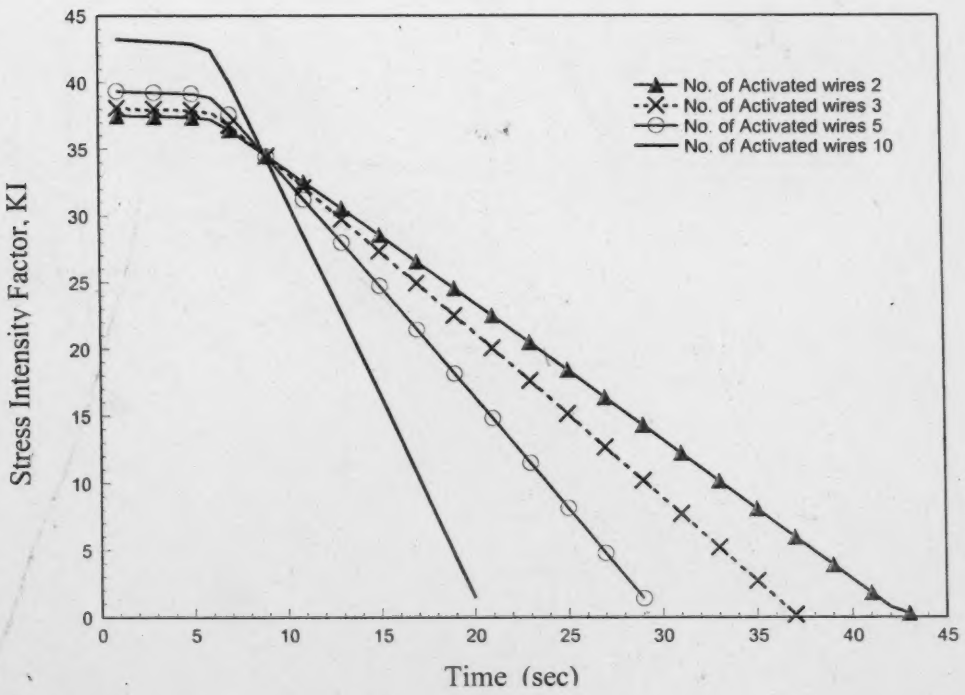

Figure 4.14: Temperature difference of the wire versus stress intensity factor at different number of activated wires.

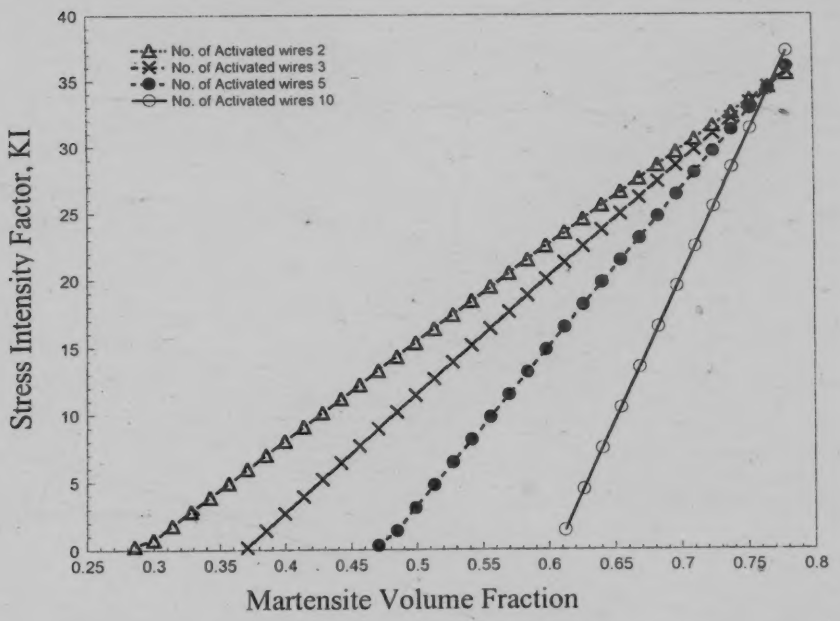

Figure 4.15: Average martensite volume fraction of the wires versus stress intensity factor for different number of activated wires.

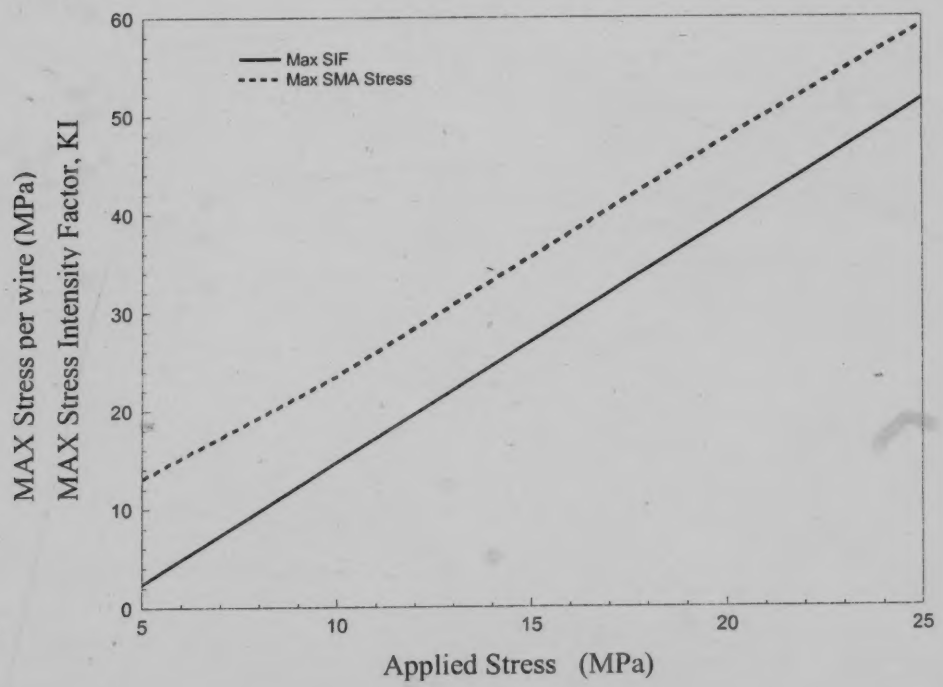

Figure 4.16: Maximum SIF and stress per wire versus applied stresses.

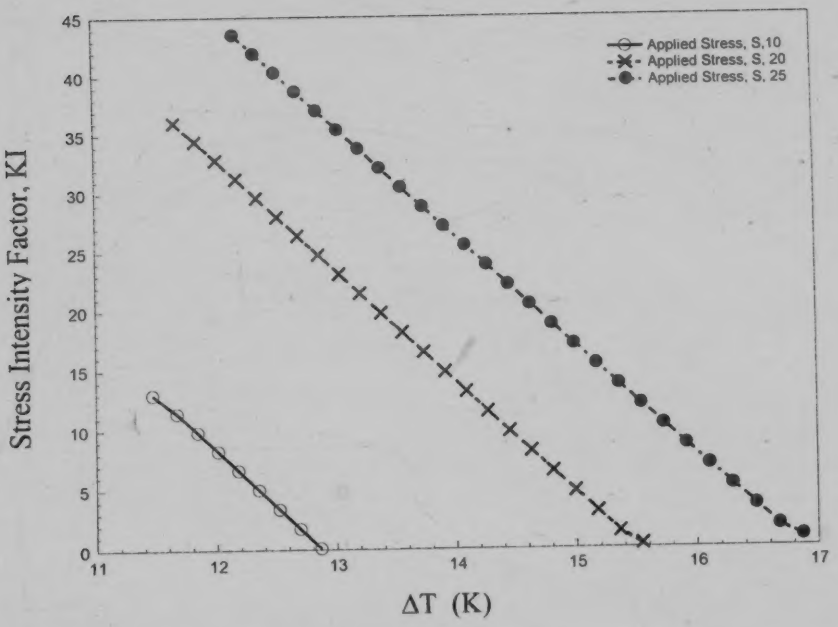

Figure 4.17: Temperature difference of the wires versus stress intensity factor for different applied stress.

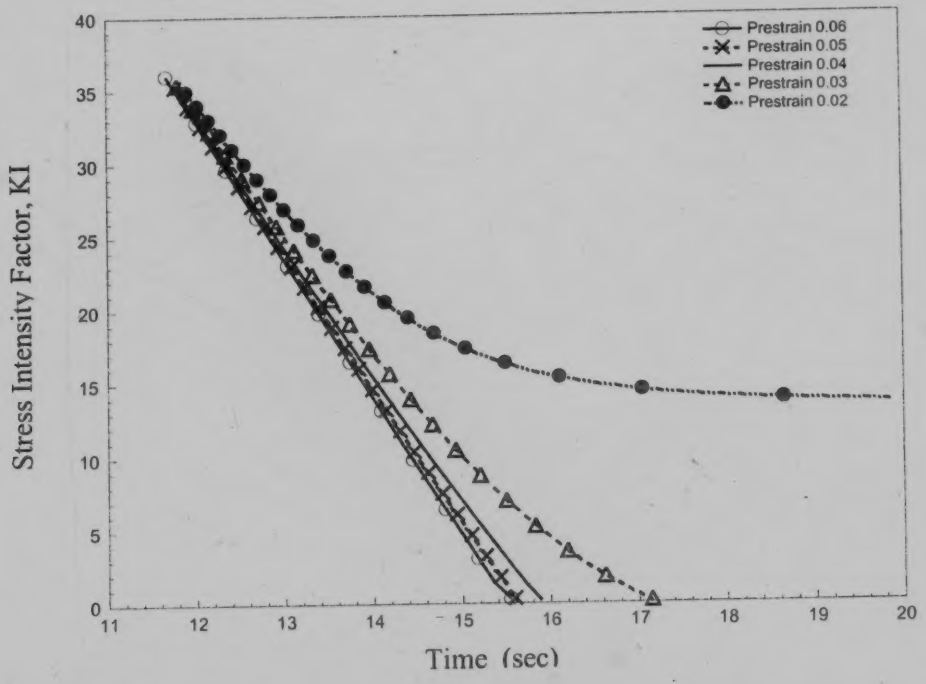

Figure 4.18: Time versus stress intensity factor for different wire prestrain.

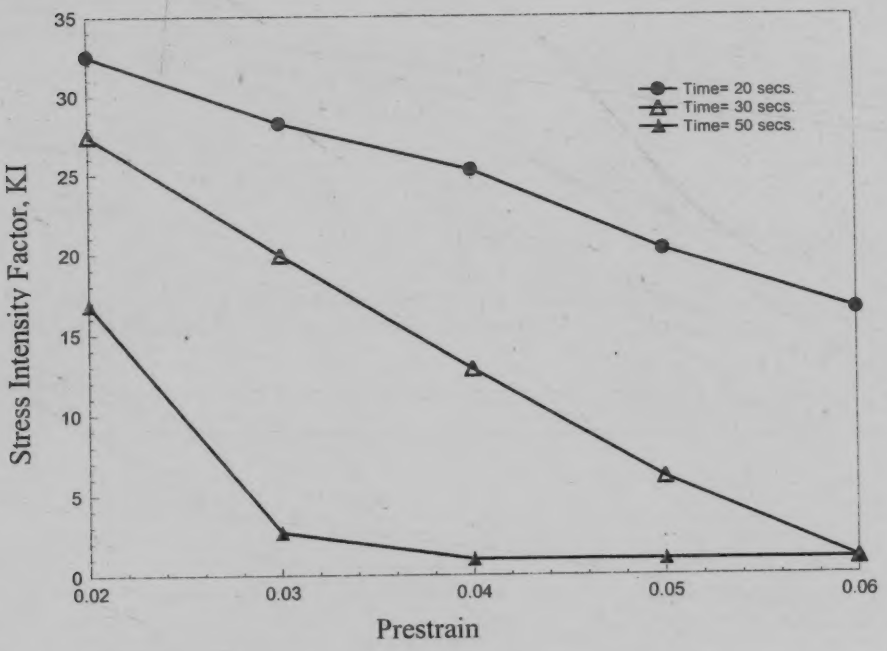

Figure 4.19: Effect of increasing SMA wire prestrain on the SIF after different times.

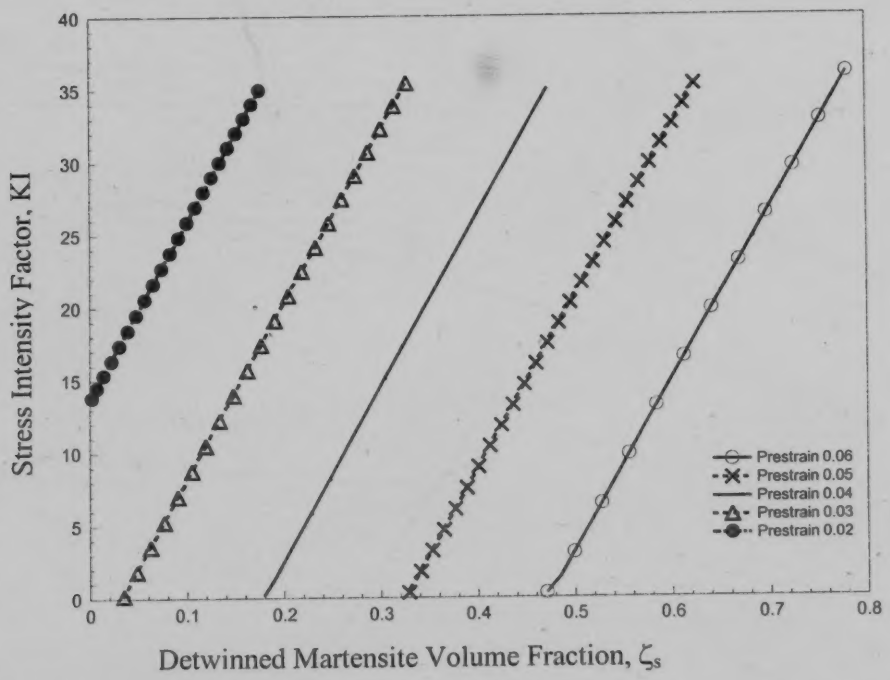

Figure 4.20: Martensite volume fraction of the wires versus stress intensity factor for different wire prestrains.

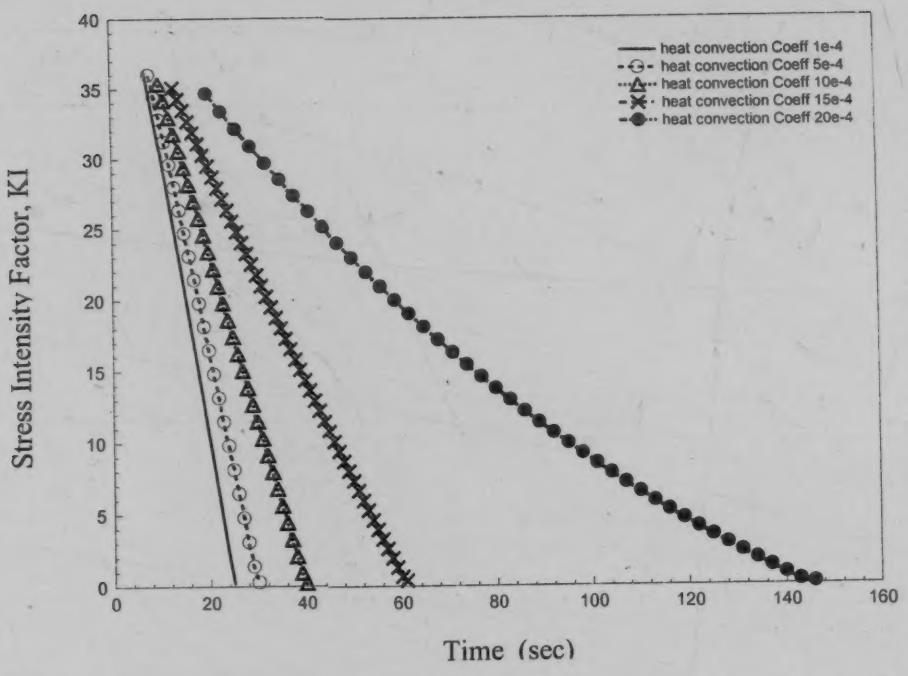

Figure 4.21: Time versus stress intensity factor at different heat convection coefficients.

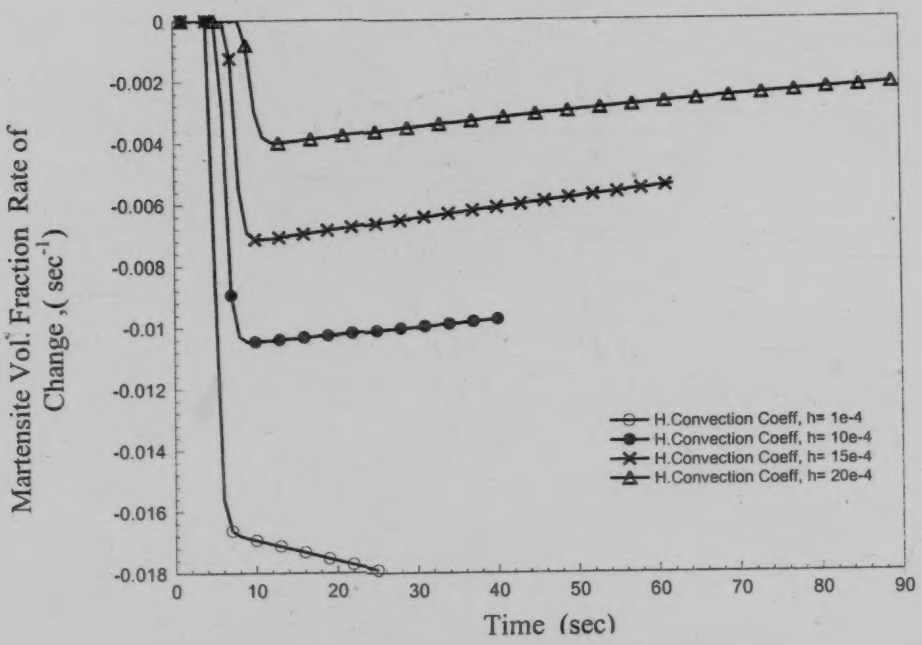

Figure 4.22: Time versus stress intensity factor at different heat convection coefficients.

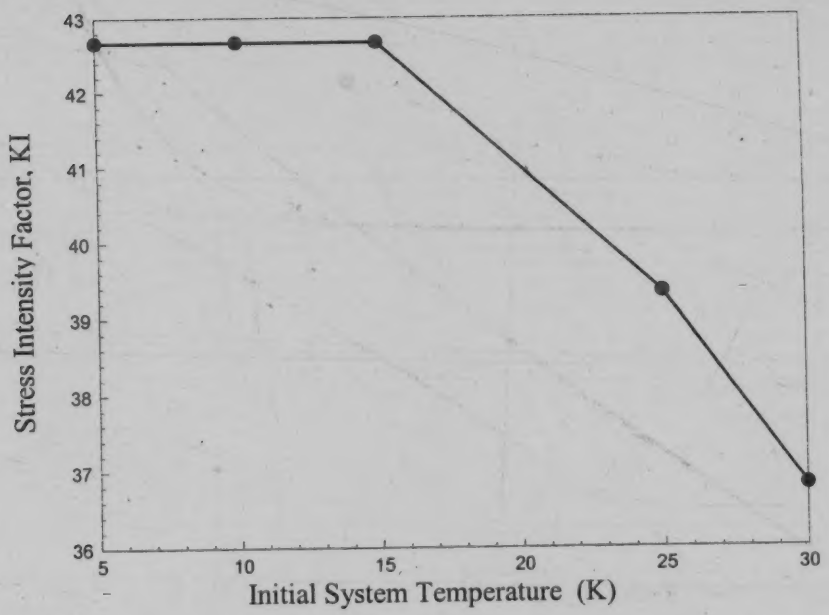

Figure 4.23: Initial system's temperature versus stress intensity factor.

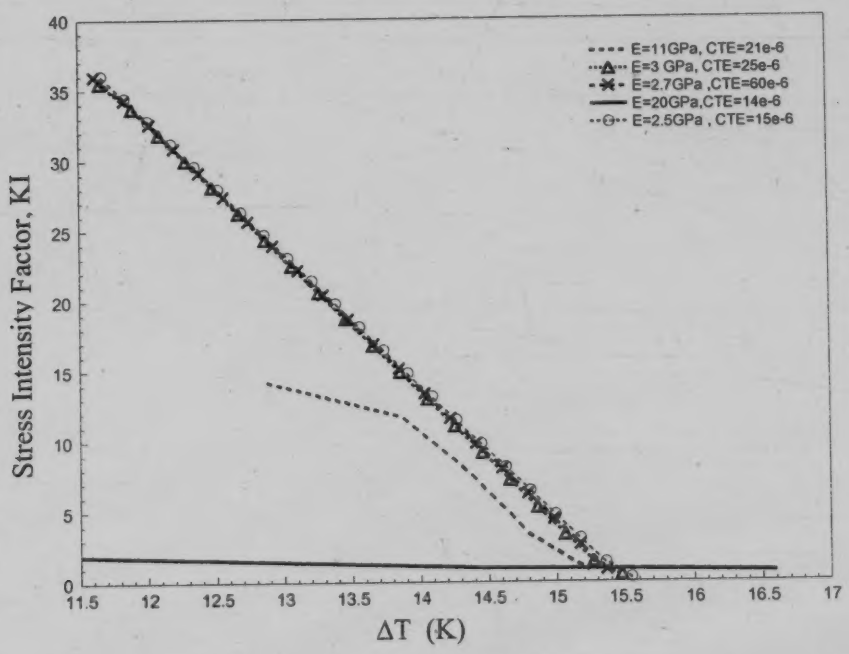

Figure 4.24: Temperature difference of the wires versus stress intensity factor for different matrix materials.

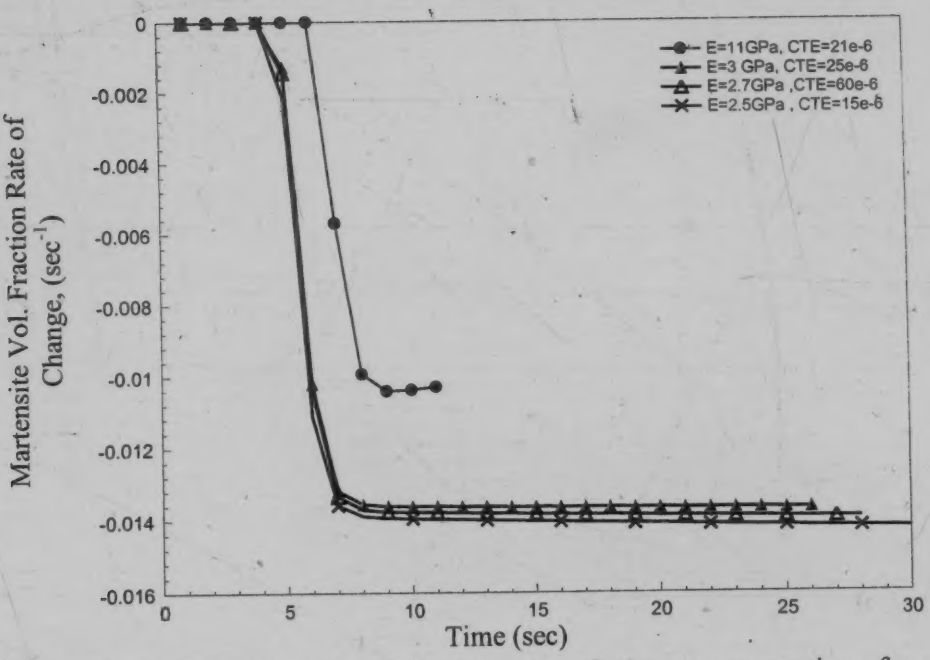

Figure 4.25: Martensite volume fraction rate of change versus time for different materials.

5. Conclusions and Future Work

5.1 Conclusions

The main aim of this research was to develop a general finite element procedure for modeling smart systems applications containing SMA components. Based on our literature survey (refer Sec 2.4) it was clear that while there was considerable work done towards finite element modeling of SMA behavior, many researchers have overlooked considering modeling multi-field loading of SMA components. This can lead to reduced effectiveness in the design tools available for SMA smart systems applications especially those require the interaction of components operating on different physical domains. Hence, there was a need to develop a generalized finite element procedure to model applications containing SMAs subjected to multi-field (i.e. electro-thermo-structural) loading and boundary conditions. Also, due to the diversity in the available SMA constitutive and material evolution relations in literature, providing that certain relations could be more accurate in modeling some applications than others, any procedure in order to be general should be flexible to adapt to different relations. This is precisely what we dealt with in this thesis.

The main characteristics of the finite element procedure that we introduced in the first phase of research are:

1- The approach to the proposed procedure was reached by coupling nonlinear structural and nonlinear transient electro-thermal procedures through the martensite volume fraction of the SMA.

2- The main characteristics of the proposed procedure is its suitability for modeling multiphysics applications (e.g. subjected to electro-thermo-structural loading and boundary conditions) that incorporate SMA components.

3- The ability to easily accommodate a variety of SMA constitutive and kinetic models..

4- Able to model various types of nonlinearity whether they're due to large deformations or due to SMA material functions (e.g. can accept SMA young's modulus even if it is function in temperature, stress and martensite volume fraction).

5- Since its structure depends on separate modules, the proposed procedure can easily be extended to simulate 2-D and 3-D problems and different geometries (i.e. by using the appropriate kinematics relations), and can be linked to commercial finite element packages to add to it the feature of modeling SMA problems.

6- The proposed procedure is believed to be an effective tool for modeling SMA applications especially with the increased MEMS and biomedical applications that depends on SMA as a main component.

The procedure was validated by comparing experimental and numerical results obtained from literature with results of the finite element procedure. The validation showed that the proposed procedure is reliable for modeling the behavior of SMA due to multi-field loading, and in modeling the pseudoelasticity and shape memory behavior of the SMA.

The second component of the research involved utilizing the proposed procedure to simulate SMA smart composite application. The application proposed in this portion of the research is a self-damage control SMA-composite smart system. The study aimed at investigating the effect of changing various parameters of the smart system on its crack closing efficiency, and hence, characterizing the performance of the smart system.

The major conclusions of the parametric study are as follow:

1- The density of the current running through the wires shouldn't exceed a maximum allowable value, to avoid adding high heat power to the system, and shouldn't be lower than a lower limit (2 amp/ mm^2 in our case) to avoid incomplete crack recovery.

2- Increasing the number of actuated wires speeds up the crack recovery process, decreases the maximum force required by each wire and increases the system sensitivity to small cracks.

3- By increasing wire diameters at constant power input, heat loss by conduction at the surface of the wires becomes the dominant effect on the recovery process, therefore, more time will be needed to recover the crack as the wires diameters are increased

4- It is suggested that heat convection with the surroundings be taken into consideration during system actuation, high surrounding heat convection coefficients might make the system reach steady state heat transfer at temperature lower than SMA transformation temperatures which might stop the crack closing process.

5- Modulus of elasticity of the matrix material has the major effect on the crack recovery process. The higher the modulus of elasticity increases the faster the recovery process.

6- The SMA wires used should have austenite start temperature close to the system's operating temperature. Otherwise, the CTE forces effect might fail the system before transformation starts.

7- Insufficient wire prestraining, might lead to insufficient SMA recovery forces, which might lead to slow and incomplete crack closing process.

8- As stresses applied on the system increases, higher wire temperature difference will be needed to recover the crack.

5.2 Future Work

The research's two major components have been concerned with finite element Modeling of SMAs and application. The finite element model can be further utilized to model SMA thin films (i.e. 2-D) and SMA solids (i.e. 3-D), which when done will prove the efficiency of the proposed procedure as a tool in the design and implementation of SMA in various configurations in smart structures. Since the proposed procedure is a generalized approach, various SMA constitutive and kinetic relations and various SMA evolution-of-properties functions can be tested to accurately describe the behavior of the SMA component in certain application. Also, the procedure can be extended to include dynamic analyses; this will improve the quality of the procedure as a general tool for modeling various SMA smart systems that might be actuated at high frequencies.

The second component of the research dealt with using the proposed procedure as a tool to help investigating the behavior of SMA composite. While our research

concentrated on studying the effect of changing various parameters on the performance of the smart system, a Neural Network could be developed by utilizing the above mentioned procedure to find more data points for each of the studied cases in the parametric study. The system's processor to estimate the optimum actuation configuration of the system for certain cracks can use this Neural Network.

Also, the procedure can be used to help investigating the effect of additional parameters on the system configuration such as the effect of the having non-uniform distribution of the actuating wires or the effect of having convection or conduction instead of isothermal boundary conditions at the end of the wires. The study can be extended to consider having more than one crack with different orientations. The data thus obtained can be used to obtain better Neural Network for estimating the proper actuation configurations needed for various problems.

Bibliography

Pence T. J., Grummon D. S. and Ivshin Y., 1994 A Macroscopic Model for Thermoelastic Hysteresis in Shape-Memory Materials AMD-Vol. 189/PVP-Vol. **292**, Mechanics of Phase Transformations and Shape Memory Alloys, 45-58 , ASME,.

Graesser E. J. and Cozzarelli F. A. 1991 Extension of a One-Dimensional Model of Hysteresis to Three Dimensions: Procedure and Verification, High Temperature Constitutive Modeling : Theory and Application, ASME, MD- **26**/AMD Vol. 121, 365-381.

Graesser E. J., 1990 Multi-Dimensional Modeling of Hysteretic Materials Including Shape Memory Alloys: Theory and Experiment, Ph.D. dissertation, State University of New York at Buffalo, NY.

Kafka V., Inelastic Mesomechanics, 1987, Singapore, New Jersey, Hong Kong: World Scientific Publ. Co..

Kafka V., 1994 Shape Memory: A New Concept of Explanation and of Mathematical Modeling. Part I: Micromechanical Explanation of the Causality in the SM Processes, Journal of Intelligent Material Systems and Structures, .**5**, November, 809-814.

Kafka, V., 1994 Shape Memory: A New Concept of Explanation and of Mathematical Modeling. Part II: Mathematical Modeling of the SM Effect and of Pseudoelasticity, Journal of Intelligent Material Systems and Structures, **5**, November, 815-824.

Müller I., 1979 A Model for a Body with Shape Memory, Arch. Rational Mech. Anal., **70**: 61-77..

Müller I. and Wilmanski,K., 1980. A Model for Phase Transformation in Pseudoelastic Bodies, Il Nuovo Cimento, **57B**, 238-318.

Müller I., 1989 On the Size of the Hysteresis in Pseudoelasticity, Continuum Mech. Thermodyn., . **1**, 125-142.

Müller I., 1991 and Xu, H., On the Pseudo-Elastic Hysteresis, Acta Metall. Mater., .**39**, 263-271.

Amalraj J, Bhattacharya A and Faulkner M G 2000 finite element modeling of phase transformation in shape memory alloy wires with variable material properties *Smart Mater. Struct.* **9** 622-631

Bathe Klaus-Jurgen 1996 Finite element procedures 5th edn. (Prentice-Hall press)

Amalraj J, 1999 Effect of variable material properties on purely thermal phase transformation in SMA wires MSc Dissertation *Dept. of Mech. Eng. University of Alberta*

Brinson L C and Lammering R 1993 Finite element analysis of the behavior of shape memory alloys and their applications *Int. J. Structures* **30** 3261-3280

Leo P H, Shield T W and Bruno O P 1993 Transient heat transfer effects on the pseudoelastic behavior of shape-memory wires *Acta metal. Mater.* **41** 2477-2485

Stoilov V, Iliev O and Bhattacharya A 2000 A moving boundary finite element method-based numerical approach for the solution of one-dimensional problems in shape memory alloys *Comput. Methods Appl. Mech.* **190** 1741-1762

Bhattacharya A, Stoilov V and Iliev O 2000 Evaluation of structural influence on performance of shape memory alloy linear actuators by sharp phase front-based constitutive models *Computational Materials Science* **18** 269-282

Trochu F and Qian Y 1997 Nonlinear finite element simulation of superelastic shape memory alloy parts *Computers & Structure* **62** 799-810

Wu W, 1996 Modeling and analysis of one and two dimensional shape memory alloy-elastomer actuators PhD Dissertation *Dept. of Mech. Eng. University of Nevada*

Brinson L C and Huang M 1996 Simplification and comparisons of shape memory alloy constitutive models *J. of Intell. Material Sys. & Struct.* **7** 108-114

Rebelo N and Hibbitt M P Finite element analysis for the design of nitinol medical devices

Brinson L C 1993 One-dimensional constitutive behavior of shape memory alloys: Thermomechanical derivation with non-constant material functions and redefined martensite internal variable *J. of Intell. Material Sys. & Struct.* **4** 229-242

Tang W and Sandstrom R 1995 Limitations of constitutive relations for TiNi shape memory alloys *Journal De Physique* **5** 185-191

Stalmans R, Humbeeck J V and Delacy L 1995 Thermodynamic modeling of shape memory behavior: Some Examples *Journal de Physique* **5** 203-209

Lu Z K and Weng G J 1997 Martensitic transformation and stress-strain relations of shape memory alloys *J. Mech. Phys. Solids* **45** 1905-1928

Tobushi H, Tanaka K, Hori T, Sawada T and Hattori T 1993 Pseudoelasticity of TiNi shape memory alloy (Dependence on maximum strain and temperature) *JSME Intl. J.* **36** 314-318

Spies R D 1996 An algorithm for simulating the isothermal hysteresis in the stress-strain laws of shape memory alloys 1996 *J. of Material Science* **31** 6631-6636

Dolce M and Cardone D 2001 Mechanical behavior of shape memory alloys for seismic applications 1.Martenisite and austenite NiTi bars subjected to torsion *Int. J. of Mech. Sciences* **43** 2631-2656

Dolce M and Cardone D 2001 Mechanical behavior of shape memory alloys for seismic applications 2.Austenite NiTi wires subjected to tension *Int. J. of Mech. Sciences* **43** 2657-2677

Boyd J G and Lagoudas D C 1996 A thermodynamical constitutive model for shape memory materials part I. The monolithic shape memory alloy *International J. of Plasticity* **12** 805-842

Abeyaratne R, Kim S and Knowles J 1994 A one-dimensional continuum model for shape-memory alloys *Int. J. Solids Structures* **31** 2229-2249

Lagoudas D C and Bhattacharya A 1998 Modeling of thin layer extensional thermoelectric SMA actuators *Int. J. Solids Structures* **35** 331-362

Bhattacharya A and Lagoudas D C 1997 A stochastic thermodynamic model for the gradual thermal transformation of SMA polycrystals *Smart Mater. Struct.* **6** 235-250

Lagoudas D C, Bo Z and Bhattacharya A 1996 A thermodynamic constitutive model for gradual phase transformation of SMA materials *SPIE* **2715** 482-493

Liang C and Rogers C A 1997 One-dimensional Thermomechanical constitutive relations for shape memory materials *J. of Intell. Material Sys. & Struct.* **8** 285-302

Tanaka K, Hayashi T, Itoh Y and Tobushi H 1992 Analysis of Thermomechanical behavior of shape memory alloys *Mechanics of Materials* **13** 207-215

Auricchio F and Sacco E A temperature-dependent beam for shape-memory alloys: constitutive modeling, finite-element implementation and numerical simulations *Comput. Methods Appl. Mech. Engrg.* **174** 171-190

Levitas V I, Idesman A V and Stein E 1999 Shape memory alloys: Micromechanical modeling and numerical analysis of structures *J. of Intell. Material Sys. & Struct.* **10** 983-996

Juhasz L, Andra H and Hesebeck O 2000 Simulation of the Thermomechanical behavior of shape memory alloys under multi-axial non-proportional loading (In Smart Structures and Materials 2000) *SPIE* **3992** 484-495

Tarabarin, S. New suture material for deep wounds of parenchymal organs. Conf. Proc.: Superelastic Shape Memory Implants in Medicine: 217-218; Tomsk, November 24-26; 1995.

Aliev, F.; Kecherukov, A.; Bychkov, B. The ambulatory compressive hemorroidectomy. Shape Memorizing Implants, Tomsk, #3: 25-26; 1992.

Mirgazizov, M.; Shamsutdinov, N.; Khafizov, R.; Saleeva, G. Experimental and morphologic basic of implants with imitators of periodontal ligaments from SMA. Conf. Proc.: Superelastic Shape Memory Implants in Medicine: 125-126; Tomsk, November 24-26; 1995.

Gjunter, V.; Itin, V.; Hodorenko, V. Shape memory implants in ophthalmology Shape Memorizing Implants, Tomsk, , #3, p. 58-59; 1992.

Lu ZK Weng GJ 2000 Two-level micromechanical theory for a shape-memory alloy reinforced composite *International-Journal-of-Plasticity* **16** 1289-1307.

Zhang W Davis M Koratkar N 2002 Energy absorbent composites featuring embedded shape memory alloys Proceedings of SPIE The-International Society for Optical Engineering399-409.

Parlinska M Clech H Balta JA Michaud V Bidaux JE Manson J Gotthardt R 2001 Adaptive composites with embedded shape memory alloys *Journal-De-Physique* **4** 4197-4204.

Ostachowicz W Kaczmarczyk S 2001 Vibrations of composite plates with SMA fibres in a gas stream with defects of the type of delamination *Composite Structures* **54** 305-311.

Sanders B Martin C Cowan D 2001Aerodynamic and aeroelastic characteristics of the DARPA Smart Wing Phase II wind tunnel model *Proceedings of SPIE The International Society for Optical Engineering* **4332** 390-398.

Choi YK Salvia M 2001 Manufacture, experimental and theoretical evaluation of adaptative glass epoxy composites with embedded shape memory alloys wires *Proceedings of SPIE The International Society for Optical Engineering* 4333 366-376.

Prahlad Harsha Chopra Inderjit 2000 Development of an adaptive flexbeam for rotorcraft applications using embedded Shape Memory Alloy (SMA) *Structural Dynamics and Materials Conference* **2** 248-261.

DeBlonk BJ Kurdila J Lagoudas C Webb G 1995 Identification of the transient response of SMA embedded flexible rods *Proceedings of SPIE The International Society for Optical Engineering* **2443** 349-359.

Bidaux E Bataillard L Manson A Gotthardt R 1993 Phase transformation behavior of thin shape memory alloy wires embedded in a polymer matrix composite *Journal De Physique* 3 561-564.

Simpson J Boller C 2002 Performance of SMA-reinforced composites in an aerodynamic profile *Proceedings of SPIE The International Society for Optical Engineering* **4698** 416-426.

Michaud V Schrooten J Parlinska M Gotthardt R Bidaux JE 2002 Shape memory alloy wires turn composites into smart structures Part II: Manufacturing and properties *Proceedings of SPIE The International Society for Optical Engineering* **4698** 406-415.

Schrooten J Michaud V Zheng Y Balta JA Manson JA 2002 Shape memory alloy wires turn composites into smart structures Part I: Material requirements *Proceedings of SPIE The International Society for Optical Engineering* **4698** 395-405.

Sittner P Michaud V Schrooten J 2002 Modelling and material design of SMA polymer composites *Materials Transactions* **43** 984-993.

Schrooten J Michaud V Parthenios J Psarras C Galiotis C Gotthardt R Manson JA Van HJ 2002 Progress on composites with embedded shape memory alloy wires *Materials Transactions* **43** 961-973.

Lau T Chan L Shi Q Zhou M 2002 Debond induced by strain recovery of an embedded NiTi wire at a NiTi/epoxy interface: Micro-scale observation Materials and Design **23** 265-270.

Parlinska M Clech H Balta JA Michaud V Bidaux JE Manson AE Gotthardt R 2001 Adaptive composites with embedded shape memory alloys *Journal De Physique* **11**

4197-4204.

Zheng Y Cui L Li Y Stalmans R 2001 Partial transformation behavior of prestrained TiNi fibers in composites *Materials Letters* **51** 425-428.

Krstulovic ON Wriggers P Krstulovic OL 2001 Self-actuating fiber composites for auto-adaptive structures *Proceedings of SPIE The International Society for Optical Engineering* **4330** 416-425.

Boller C Konstanzer P Matsuzaki Y Ikeda T 2001 Damping in SMA-reinforced composites using SMA-intrinsic properties *Proceedings of SPIE The International Society for Optical Engineering* **4332** 471-479.

Balta JA Michaud V Parlinska M Gotthardt R Manson JAE 2001 Adaptive composites with embedded NiTiCu wires *Proceedings of SPIE The International Society for Optical Engineering* **4333** 377-386.

Schrooten J Tsoi KA Stalmans R Zheng Y Sittner P 2001 Comparison between generation of recovery stresses in shape memory wires and composites: Theory and reality *Proceedings of SPIE The International Society for Optical Engineering* **4234** 114-124.

Sittner P Stalmans R 2000 Developing hybrid polymer composites with embedded shape-memory alloy wires *JOM* **52** 15-20.

Lurie SA Efimov DA Poluhina NO 2000 Special feature of the SMA composite materials deformation *Proceedings of SPIE The International Society for Optical Engineering* **3992** 451-462.

Bruck HA Moore CL 1999 Mechanical characterization of shape memory alloy composites for designing smart structures *American Society of Mechanical Engineers, Aerospace Division* **59** 99-103.

Jonnalagadda KD Sottos NR Qidwai MA Lagoudas C 1997 Transformation of embedded shape memory alloy ribbons *Proceedings of SPIE The International Society for Optical Engineering* **3039** 242-253.

Wei ZG Tang CY Lee WB 1997 Design and fabrication of intelligent composites based on shape memory alloys *Journal of Materials Processing Technology* **69** 68-74.

Giurgiutiu V Rogers CA Zuidervaart J 1997 Incrementally adjustable rotor-blade tracking tab using SMA composites *Structural Dynamics and Materials Conference* **2** 1456-1466.

Berman JB White SR 1996 Theoretical modelling of residual and transformational stresses in SMA composites *Smart Materials and Structures* **5** 731-743.

Sottos R Kline GE Qidwai MA Lagoudas C 1996 Analysis of phase transformation fronts in SMA composites Proceedings of SPIE The International Society for Optical Engineering. **2715** 427-438.

Hebda A White R 1995 Structural behavior of SMA composite beams *Adaptive Material Systems American Society of Mechanical Engineers, Applied Mechanics Division, AMD* **206** 111-119.

Hebda DA Whitlock ME Ditman JB White SR 1995 Manufacturing of adaptive graphite/epoxy structures with embedded nitinol wires *Journal of Intelligent Material Systems and Structures* **6** 220-228.

Bidaux JE Bataillard L Manson JA Gotthardt R 1993 Phase transformation behavior of thin shape memory alloy wires embedded in a polymer matrix composite *Journal De Physique* **3** 561-564.

White SR Whitlock ME Ditman JB Hebda DA 1993 Manufacturing of adaptive graphite/epoxy structures with embedded Nitinol wires *Adaptive Structures and Material Systems American Society of Mechanical Engineers, Aerospace Division* **35** 71-79.

Saunders WR Robertshaw HH Rogers CA 1991 Structural acoustic control of a shape memory alloy composite beam *J Intell Mater Syst Struct* **2** 508-527.

Liang C Rogers CA Fuller CR 1991 Acoustic transmission and radiation analysis of adaptive shape memory alloy reinforced laminated plates *J Sound Vib* **145** 23-41.

Paine JS Rogers CA 1995 Shape memory alloys for damage resistant composite structures *Proceedings of SPIE The International Society for Optical Engineering* **2427** 358-371.

http://smart.tamu.edu

Wei ZG, Tang CY, Lee WB, "Design and fabrication of intelligent composites based on shape memory alloys" Journal of Materials Processing Technology, 1997, 69 68-74.

Byung K; Xu Y; Oishi R; Nagai H; Yoshida H; Akimune Y; Otsuka K; Kishi T, "Thermomechanical characterization and development of SMA embedded CFRP composites with self-damage control", Proceedings-of-SPIE-The-International-Society-for-Optical-Engineering, 4699, 2002 p 182-190.

Wang X, "Shape memory alloy volume fraction of pre-stretched shape memory alloy wire-reinforced composites for structural damage repair" Smart-Materials-and-Structures. v 11 n 4 August, p 590-595

Appendix

A1- Expressions of the Symbols in Equation (3.2):

The Linear stiffness matrix for *m* number of elements is given by (Bathe, 1996),

$$ {}^{t}K_{L}^{(i-1)} = \sum_{m} \int_{V} {}^{t}\mathrm{B}_{\mathrm{L}}^{(m)(i-1)\mathrm{T}} \; {}^{t}\mathrm{C}^{(m)(i-1)} \; {}^{t}\mathrm{B}_{\mathrm{L}}^{(m)(i-1)} \, dV , $$

where ${}^{t}\mathrm{B}_{\mathrm{L}}$ is the kinematics relations' matrix. This matrix relates the strain to the displacement of the nodes; and it depends on the geometry of the model. Since large deformations are assumed the geometry is assumed to be changing over the time, therefore, the kinematics relations' matrix is changing with time as well.

The Nonlinear stiffness matrix for *m* number of elements is given by (Bathe, 1996),

$$ {}^{t}K_{NL}^{(i-1)} = \sum_{m} \int_{V} {}^{t}\mathrm{B}_{\mathrm{NL}}^{(m)(i-1)\mathrm{T}} \; {}^{t}\mathrm{S}^{(m)(i-1)} \; {}^{t}\mathrm{B}_{\mathrm{NL}}^{(m)(i-1)} \, dV , $$

note that the nonlinear part of the stiffness matrix is dependent of the stress configuration of the system. The internal forces due to stress vector is,

$$ {}^{t}F_{\phi}^{(i-1)} = \sum_{m} \int_{V} {}^{t}\mathrm{B}_{\mathrm{L}}^{(m)(1-1)\mathrm{T}} \; {}^{t}\hat{\mathrm{S}}^{(m)(i-1)} \, dV , $$

This vector represents the internal forces in generated in the structure as a reaction to the externally applied force. The both are balanced in reality, but as a result of linearization of the Green-Lagrange equation, the finite element solution gives out of balance between of these two forces. With the aid of the iterative solution procedure introduced in the dissertation, this out of balance is minimized.

The Externally applied forces vector, which could also include any concentrated or dynamic loads,

$$^{t+\Delta t}\Re = \int_{^oV} H^T\, {}^{t+\Delta t}f^B \; dV + \int_{^oS} H^{S^T}\, {}^{t+\Delta t}f^S \; dS \;,$$

this vector include the body forces vector (first term) in addition to the surface traction forces(second term). This vector can also include the dynamic effects represented in the inertia forces.

A2- Derivation of the term $^tC_{ijrs}$ using Brinson (1993) modified constitutive and kinetic relations:

Starting from SMA constitutive relation introduced by Tanaka (1986),

$$\sigma - \sigma_o = D(\xi)\varepsilon - D(\xi_o)\,\varepsilon_o + \Omega(\xi)\,\xi_s - \Omega(\xi_o)\,\xi_{so} + \alpha\,(\theta - \theta_o), \qquad \text{(A2-1)}$$

some authors (e.g. Brinson and Lammering, 1993) suggested that the stress-temperature vector, α, be constant since it is very small compared to other terms. Also, the same authors suggested that the transformation tensor, Ω, be a function of the martensite volume fraction. Differentiating the relation in (A2-1) with respected to strain,

$$\frac{\partial \sigma}{\partial \varepsilon} = \frac{\partial}{\partial \varepsilon}\left(D(\xi)\varepsilon\right) + \frac{\partial}{\partial \varepsilon}\left(\Omega(\xi)\,\xi_s\right), \qquad \text{(A2-2)}$$

the first term of (A2-2) could be further chain-differentiated to get:

$$\frac{\partial}{\partial \varepsilon}\left(D(\xi)\varepsilon\right) = \frac{\partial D(\xi)}{\partial \varepsilon}\,\varepsilon + D(\xi) = \frac{\partial D(\xi)}{\partial \xi}\frac{\partial \xi}{\partial \sigma}\frac{\partial \sigma}{\partial \varepsilon}\,\varepsilon + D(\xi)$$

$$= \left(D_m - D_a\right)\frac{\partial \xi}{\partial \sigma}\frac{\partial \sigma}{\partial \varepsilon}\,\varepsilon + D(\xi), \qquad \text{(A2-3)}$$

chain differentiation of the second term of (A2-2) gives:

$$\frac{\partial}{\partial \varepsilon}\left(\Omega(\xi)\,\xi_s\right) = \frac{\partial}{\partial \varepsilon}\left(-\varepsilon_L D(\xi)\,\xi_s\right) = \left(D_m - D_a\right)\frac{\partial \xi}{\partial \sigma}\frac{\partial \sigma}{\partial \varepsilon} + \frac{\partial \xi_s}{\partial \sigma}\frac{\partial \sigma}{\partial \varepsilon}\,, \qquad \text{(A2-4)}$$

substituting (A2-3) and (A2-4) in (A2-2) and simplifying gives the expression in Equation (3.7).

A3- Derivation of $\left[\begin{array}{cc} \frac{\partial \xi}{\partial \sigma} & \frac{\partial \xi_s}{\partial \sigma} \end{array}\right]$ for different types of SMA transformation

Transformation to detwinned martensite above martensite-start temperature expressions is given in Equations (3.10) to (3.12). To derive the same expressions for transformation to detwinned martensite below the martensite-start temperature the transformation to detwinned martensite below the martensite-start temperature relations are differentiated with respect to stress as follow:

For the stress induced martensite,

$$\xi_s = \frac{1-\xi_{so}}{2}\cos\left\{\frac{\pi}{\sigma_s^{cr}-\sigma_f^{cr}}[\sigma-\sigma_f^{cr}]\right\}+\frac{1+\xi_{so}}{2} \quad , \tag{A3-1b}$$

and for the thermally induce martensite,

$$\xi_\theta = \xi_{\theta_0} - \frac{\xi_{\theta_0}}{1-\xi_{so}}(\xi_s-\xi_{so})+\Delta_\theta \ , \tag{A3-2b}$$

where, $\Delta_\theta = \frac{1-\xi_{\theta_0}}{2}\cos\left\{\frac{\pi}{\sigma_s^{cr}-\sigma_f^{cr}}[a_M^{\circ}(\theta-M_f)+1]\right\}$ for $M_f < \theta$, Else $\Delta_\theta = 0$,

therefore,

$$\frac{\partial \xi_s}{\partial \sigma} = -\frac{\pi}{\sigma_s^{cr}-\sigma_f^{cr}}\frac{1-\xi_{so}}{2}\sin\left\{\frac{\pi}{\sigma_s^{cr}-\sigma_f^{cr}}[\sigma-\sigma_f^{cr}]\right\}. \tag{A3-3b}$$

The kinetic relations for the transformation to austenite are also differentiated with respect to stress to get $\left[\begin{array}{cc} \frac{\partial \xi}{\partial \sigma} & \frac{\partial \xi_s}{\partial \sigma} \end{array}\right]$ expressions at this case, the differentiation process gives:

$$\frac{\partial \xi}{\partial \sigma} = \frac{a_A}{C_A}\frac{\xi_{so}}{2}\left\{\sin\left[a_A(\theta-A_s-\frac{\sigma}{C_A})\right]+1\right\} \tag{A3-1c}$$

$$\frac{\partial \xi_s}{\partial \sigma} = \frac{\xi_{s0}}{\xi_o} \frac{\partial \xi}{\partial \sigma} \qquad \text{(A3-2c)}$$

$$\frac{\partial \xi_\theta}{\partial \sigma} = \frac{\xi_{\theta 0}}{\xi_o} \frac{\partial \xi}{\partial \sigma} \qquad \text{(A3-3c)}$$

The derived expressions are used to find the stress-strain relation matrix **C** according the transformation phase of the SMA at specific time.

A4- Expressions of the Symbols in Equation (3.14):

The terms of the discreticized energy-balance equation for m number of elements are given as follow:

The conduction part is given by:

$$^{t+\Delta t}K^{k(i-1)} = \sum_m \int_{V^{(m)}} B^{(m)T} \; ^{t+\Delta t}k^{(m)(i-1)} \; B^{(m)} \, dV^{(m)},$$

where B is the temperature gradient vector at the nodes, and k is thermal conductivity vector of each element. The heat generation due to conduction heat transfer matrix is given by,

$$^{t+\Delta t}Q^{k(i-1)} = \sum_m \int_{V^{(m)}} B^{(m)T} [\; ^{t+\Delta t}k^{(m)(i-1)} \; B^{(m)} \; ^{t+\Delta t}\theta^{(i-1)}] \, dV^{(m)}.$$

The convection terms are given by,

$$^{t+\Delta t}K^{c(i-1)} = \sum_m \int_{S_c^{(m)}} ^{t+\Delta t}h^{(m)(i-1)} \cdot H^{S(m)T} H^{S(m)} \, dS_c^{(m)}$$

$$^{t+\Delta t}Q^{c(i-1)} = \sum_m \int_{S_c^{(m)}} ^{t+\Delta t}h^{(m)(i-1)} \; H^{S(m)T} [H^{S(m)} \; (\; ^{t+\Delta t}\theta_c - \; ^{t+\Delta t}\theta^{S(i-1)})] \, dS_c^{(m)}$$

and the stored heat is given by,

$$^{t+\Delta t}C^{(i)} = \sum_{m} \int_{V^{(m)}} H^{(m)T} \; {}^{t+\Delta t}(\rho c)^{m(i-1)} \; H^{(m)} \, d^{o}V$$

where,

$$^{t+\Delta t}\dot{\theta}^{(i)} = \frac{^{t+\Delta t}\theta^{(i-1)} + \Delta\theta^{(i)} - {}^{t}\theta}{\Delta t}$$

A5- Kinetic relations used by Amalraj et al for modeling SMA behavior

For transformation from Martensite to Austenite the kinetic relations used are only function in temperature,

$$\xi(\theta) = \xi(A_S)\left[1 - \int_{A_S}^{\theta} G(\theta) d\theta\right]$$

where,

$$G(\theta) = \frac{1}{S_{M \longrightarrow A}\sqrt{2\pi}} \exp\left[-\frac{1}{2}\left(\frac{\theta - \frac{1}{2}(A_S + A_F)}{S_{M \longrightarrow A}}\right)^2\right]$$

and: $S_{M \longrightarrow A}$ is the standard deviation of the normal distribution $G(\theta)$. Since the above expressions are independent of stress, the C matrix at this case will be zero.

A6- SMA material evolution functions

The SMA material evolution functions used all through this dissertation are assumed to be changing linearly only with the martensite volume fraction of the SMA. This assumption is acceptable by many authors in literature (e.g. Brinson, 1993 and Amalraj et al, 1999). A summary of these relations is given as follow:

Modulus of elasticity:

$$^{t}D(\xi) = D_A - {}^{t}\xi(D_A - D_M) \qquad \text{(A6-1)}$$

Thermal conductivity:

$$^{t}k(\xi) = k_A - ^{t}\xi(k_A - k_M) \qquad \text{(A6-2)}$$

Heat Capacity:

$$^{t}C(\xi) = C_A - ^{t}\xi(C_A - C_M) \qquad \text{(A6-3)}$$

Resistivity:

$$^{t}\rho(\xi) = \rho_A - ^{t}\xi(\rho_A - \rho_M) \qquad \text{(A6-4)}$$

A7- Out-of-balance Load Vector Convergence Criterion

The convergence criterion used in the finite element procedure is obtained by measuring the out-of-balance load vector. It is required that the norm of the out-of-balance load vector be within a preset tolerence ε_F of the original load increment,

$$\left\| ^{t+\Delta t}R - ^{t+\Delta t}F \right\|_2 \leq \varepsilon_F \left\| ^{t+\Delta t}R - ^{t}F \right\|_2$$